

Common origin of θ_{13} and dark matter within the flavor symmetric scoto-seesaw framework

Joy Ganguly,^{a,b} Janusz Gluza,^c Biswajit Karmakar^{c,1}

^a*Department of Physics, Indian Institute of Technology Hyderabad, Telenagana, India*

^b*Department of BSH, University of Engineering and Management, Kolkata, India*

^c*Institute of Physics, University of Silesia, Katowice, Poland*

E-mail: joyganguly.hep2022@gmail.com, janusz.gluza@us.edu.pl,
biswajit.karmakar@us.edu.pl

ABSTRACT: To understand the observed pattern of neutrino masses and mixing as well as to account for the dark matter we propose a hybrid scoto-seesaw model based on the A_4 discrete flavor symmetry. In this setup, including at least two heavy right-handed neutrinos is essential to employ the discrete flavor symmetry that mimics once popular tribimaximal neutrino mixing at the leading order via type-I seesaw. The scotogenic contribution then acts as a critical deviation to reproduce the observed value of the reactor mixing angle θ_{13} (within the trimaximal mixing scheme) and to accommodate potential dark matter candidates, pointing towards a common origin of θ_{13} and dark matter. The model predicts the atmospheric angle to be in the upper octant, excludes some regions on the Dirac CP phase, and restricts the Majorana phases too. Further, normal and inverted mass hierarchies can be distinguished for specific values of the relative phases associated with the complex light neutrino mass matrix. Owing to the considered flavor symmetry, contributions coming from the scotogenic mechanism towards the lepton flavor violating decays such as $\mu \rightarrow e\gamma$, $\tau \rightarrow e\gamma$ vanish, and a lower limit on the second right-handed neutrino mass can be obtained. Prediction for the effective mass parameter appearing in the neutrinoless double beta decay falls within the sensitivity of future experiments such as LEGEND-1k and nEXO.

¹Corresponding author.

Contents

1	Introduction	1
2	Minimal scoto-seesaw model	4
3	Scoto-seesaw with flavor A_4 symmetry: the FSS model	5
4	Neutrino masses and mixing in the FSS model	9
5	Numerical analysis of the FSS model	12
5.1	Case I: $\phi_{AC} = \phi_{BC} = 0$	13
5.2	Case II : $\phi_{AC} = 0$	16
5.3	Case III: $\phi_{AC} = \phi_{BC} = \phi_x$	16
5.4	Case IV: $\phi_{BC} = 0$	18
5.5	General case	19
6	Phenomenological implications for the FSS model	25
7	Conclusions	30

1 Introduction

The discovery of neutrino oscillation [1–5] suggests that at least two neutrinos are massive but having very small masses with respect to the charged leptons and quarks. This situation opens up a window for interpretations which go beyond the Standard Model (SM) of particle physics. On the other hand, it is also well established that the neutrino flavor mixing is significantly large compared to the quark mixing which also demands an extension of the SM (either by particle content or symmetry extension). Another extraordinary problem in particle physics as of today is the nature of dark matter (DM), whose relic abundance is precisely measured by the WMAP [6] and PLANCK [7] satellite experiments and the existence of such DM is strongly supported by the gravitational lensing, galactic rotation curve and large scale structure of the Universe [8] as well. However, the SM of particle physics fails to provide an appropriate candidate for DM. Now, from a theoretical perspective, the origin of tiny neutrino masses can be well understood within the framework of various seesaw mechanisms. The simplest one is the type-I seesaw mechanism [9–13] where usually three singlet right-handed neutrinos are added to the SM; then three left-handed neutrinos can be massive. This “complete” sequential seesaw scenario is denoted by $(\#\nu_L, \#N_R) = (3, 3)$ where $\#$

ν_L , $\#N_R$ denote the number of generations of left-handed and right-handed neutrinos respectively. However, as first pointed out in [13], the number of right-handed neutrinos added to the SM is not fixed as they do not carry any anomaly [14]. A simpler version of the type-I seesaw is the minimal seesaw which further reduces the number of free parameters [15–17]. In the (3,2) seesaw mechanism only two right-handed neutrinos are introduced to obtain viable neutrino masses. However, the flavor structure of the relevant lepton mass matrices still remains undetermined.

The flavor structures of the lepton mass matrices and hence the observed non-trivial pattern of the lepton flavor mixing can be examined by incorporating non-Abelian discrete flavor symmetries to the SM. For this purpose discrete symmetry groups such as A_4 , S_4 , A_5 , $\Delta(27)$ are often used [18]. For a general overview and implementation of discrete symmetries in neutrino physics see [19–25]. Such discrete flavor symmetries can explain various fixed mixing schemes such as bi-maximal (BM), golden ratio (GR) and hexagonal (HG) [26–30] mixings, with the most popular one being the tri-bimaximal (TBM) mixing [31, 32]. In the TBM mixing scheme the solar and atmospheric mixing angles take values $\sin^2 \theta_{12} = 1/3$ and $\sin^2 \theta_{23} = 1/2$ respectively, whereas the reactor mixing angle is fixed at $\sin^2 \theta_{13} = 0$. Therefore, a discrete flavor symmetric construction with two right-handed neutrinos is a very economical scenario to explain neutrino masses and TBM mixing simultaneously [33–35]. Neutrino model building with two right-handed neutrinos in various limiting cases can be found in [36]. Among various discrete groups employed for this purpose, A_4 is the most popular one [37–42]. This symmetry was initially proposed as an underlying family symmetry for the quark sector. It is a discrete group of even permutations of four objects with three inequivalent one-dimensional representations (1 , $1'$, and $1''$) and a three-dimensional representation (3). Interestingly, the three generations (or flavors) of right-handed charged lepton singlets can fit into three inequivalent one-dimensional representations. Conversely, A_4 is the smallest group with a three-dimensional irreducible representation. Then three SM lepton doublets can transform together as a triplet under A_4 [39–41]. So far, so good; however, in the last decade, the reactor neutrino mixing angle θ_{13} is decisively measured [43–47] to be adequately large ($\sim 9^\circ$) and hence the era of fixed patterns (such as BM, TBM, GR, HG) of the lepton mixing matrix is over. To generate non-zero θ_{13} various approaches are considered either by additional contributions to the neutrino sector or considering additional corrections from the charged lepton sector or including corrections to vacuum alignments of the flavons etc. [48–93]. As consequence various descendants of the fixed mixing schemes have emerged. For example, even if the TBM mixing is obsolete now, two of its successors are still compatible with data. These mixing schemes are known as trimaximal mixing (TM) mixings [30, 62, 94, 95] which preserves the first (second) column of the TBM mixing matrix and are called TM_1 (TM_2) mixing, respectively.

In this work, we consider a scotogenic contribution [96] to the underlying TBM mixing scheme establishing a common origin of the nonzero θ_{13} and cosmological DM. Many radiative models

account for the tiny neutrino masses [97–101] and perhaps the simplest one is the scotogenic model which also naturally accommodates potential candidate for dark matter [96]. In the present article, we explore the idea of combining seesaw and scotogenic (termed as scoto-seesaw) model [102] to explain neutrino mass and mixing in a consistent way with well-motivated A_4 discrete flavor symmetry. *In our proposal, the nature of cosmological dark matter and reactor mixing angle θ_{13} share a unified origin.* Our full model comprises of (3,2) seesaw and then combines it with the scotogenic mechanism, which predicts three neutrinos to be massive. The Yukawa structure of the scotogenic contribution is formulated by adding flavon fields which transform non-trivially under the flavor symmetry. With this, we show that our model can successfully explain the lepton mixing with non-zero reactor angle θ_{13} and includes leptonic CP violation. Due to the flavor symmetric construction, the model is extremely predictive in nature and offers many interesting results involving neutrino mass hierarchy, octant of the atmospheric mixing angle θ_{23} and restricts the Dirac CP phase. In addition, we constrain the absolute neutrino masses and Majorana CP phases. On the other hand, the model can be falsified by null results of future neutrinoless double beta decay experiments. Interestingly, due to the specific flavor structure of the Yukawa couplings as a consequence of the flavor symmetry, the scotogenic part does not contribute in the lepton flavor violating decays such as $\mu \rightarrow e\gamma$ and only right-handed neutrinos contribute in such decays. We begin with a minimal type-I seesaw assisted by the A_4 discrete flavor symmetry, which helps reproduce the TBM mixing. The model also contains additional Z_N symmetries to forbid unwanted contributions in the lepton sector, and an inherent Z_2 symmetry also ensures the stability of the dark matter. Thanks to the considered symmetry, the charged lepton mass matrix as well as the heavy right-handed Majorana neutrino mass matrix, are diagonal to start with. Therefore, the structure of the 3×2 Dirac Yukawa matrix turns out to be solely responsible for generating the TBM mixing with two right-handed neutrinos. Now, the inclusion of the scotogenic contribution to the neutrino mass helps in reproducing the TM_2 mixing and generates the observed value of the reactor mixing angle θ_{13} . It also naturally incorporates dark matter candidates (three potential dark matter candidates, such as the dark fermion and real and imaginary components of the scalar field involved in the scotogenic contribution) into the picture.

The rest of the paper is organized as follows. In Section 2 we first describe the minimal scoto-seesaw model. Then in Section 3 we present the A_4 flavor symmetric scoto-seesaw model with two right-handed neutrinos and describe the construction of the model based on the symmetries of the framework. In Section 4 we present the correlation among the parameters involved in our analysis. We carry out the complete analysis for various limiting and general cases and present their predictions in Section 5. Then in Section 6 we mention various phenomenological implications of undertaken analysis and finally conclude in Section 7. We also included in the Appendix a short note on A_4 multiplication rules used in our analysis.

2 Minimal scoto-seesaw model

In Ref. [102], the (3,1) scenario of seesaw mechanism [12, 13, 103] and the scotogenic model [96] are combined to propose a minimal scoto-seesaw model. This model consists of only one right-handed neutrino N_R , one singlet fermion f , and one extra scalar doublet η . In addition to these particles, one Z_2 symmetry is introduced, which is responsible for the stability of the dark matter. All the standard model fields, N_R , are even under the Z_2 symmetry, while the dark sector consists of one fermion f and scalar field η which are odd under Z_2 . This proposal generates the atmospheric neutrino mass scale at the tree level with the conventional (3,1) seesaw term with N_R , and the solar neutrino mass scale is generated at a one-loop level, as a result, the hierarchy between the atmospheric and solar scale is maintained¹. With this field content, the lepton Yukawa and mass terms can be written as

$$\mathcal{L} = -Y_N^k \bar{L}^k i\sigma_2 H^* N_R + \frac{1}{2} M_R \bar{N}_R^c N_R + Y_f^k \bar{L}^k i\sigma_2 \eta^* f + \frac{1}{2} M_f \bar{f}^c f + h.c. \quad (2.1)$$

where L^k are the lepton doublets. The scalars $H = (H^+, H^0)^T$ and $\eta = (\eta^+, \eta^0)$ are the $SU(2)$ doublets. Y_N and Y_f are complex 3×1 Yukawa coupling matrices, and $M_{R,f}$ are the mass matrices for N_R and f . The total neutrino mass reads [102]

$$M_\nu^{ij} = -\frac{v^2}{M_N} Y_N^i Y_N^j + \mathcal{F}(m_{\eta_R}, m_{\eta_I}, M_f) Y_f^i Y_f^j. \quad (2.2)$$

Here the first term is due to the tree-level seesaw mechanism while the second term originates from the scotogenic correction with

$$\mathcal{F}(m_{\eta_R}, m_{\eta_I}, M_f) = \frac{1}{32\pi^2} \left[\frac{m_{\eta_R}^2 \log\left(\frac{M_f^2}{m_{\eta_R}^2}\right)}{M_f^2 - m_{\eta_R}^2} - \frac{m_{\eta_I}^2 \log\left(\frac{M_f^2}{m_{\eta_I}^2}\right)}{M_f^2 - m_{\eta_I}^2} \right], \quad (2.3)$$

where m_{η_R} and m_{η_I} are the masses of the neutral component of η [108]. However, this model predicts one massless neutrino and demands extension to explain all the neutrino oscillation data. Hence, to understand the observed pattern of neutrino masses and mixing, in the next section we will present a modified scoto-seesaw model where two right-handed neutrinos and A_4 discrete flavor symmetry will reproduce non-zero θ_{13} mixing angle and will account for the dark matter content. In Ref. [109], the authors already discussed the model with two right-handed neutrinos in the context of the scoto-seesaw scenario but with the Z_8 symmetry. As we will see, the set-up based on the A_4 flavor symmetry is substantially different in construction from the Z_8 scenario, resulting in a completely different texture of the Yukawa couplings and mass matrices. As mentioned earlier, the A_4 flavor symmetry is well motivated in reproducing the TBM mixing scheme and such symmetry

¹Earlier such hierarchy of the atmospheric and solar neutrino mass scales (and associated mixing) was explained with a type-I seesaw mechanism where the right-handed neutrinos contribute hierarchically and implemented within the frameworks of sequential dominance [16, 17, 36, 104–106] and constrained sequential dominance [59, 107]

can arise in various ways, such as starting from a continuous group [110–115] or superstring theory in compactified extra dimensions [40, 41, 116–125]. We will show that due to the presence of the A_4 symmetry with diagonal structure of the charged leptons and heavy right-handed neutrinos, the TBM mixing can be generated at the leading order in the context of the minimal type-I seesaw. Subsequently, the scotogenic contribution acts as a crucial deviation from TBM mixing to generate non-zero θ_{13} (reproducing the TM_2 mixing scheme) as well as providing essential dark matter candidates, thus unifying the origin of θ_{13} and dark matter. The A_4 symmetry assists us to obtain analytic expressions for neutrino masses and mixing angles as well as yields interesting correlations among the oscillation parameters with distinctive predictions; see section 4. In [109], the CP symmetry is spontaneously broken by the complex vacuum expectation value of the singlet field whereas in our analysis the source of CP violation is due to the complex couplings and relative values of CP phases determine the hierarchy of the masses.

3 Scoto-seesaw with flavor A_4 symmetry: the FSS model

The model which we propose is a hybrid scoto-seesaw framework with usual scotogenic fermion f and scalar doublet η , supported additionally by the A_4 discrete flavor symmetry and two right-handed neutrinos $N_{R_{1,2}}$. To obtain the flavor structure of the Yukawa couplings the flavons $\phi_s, \phi_a, \phi_T, \xi$ are introduced. The inclusion of flavon fields (SM gauge singlets) is a characteristic feature of models with discrete flavor symmetries [19–25]. In a similar manner, we also incorporate additional Z_N discrete symmetries which forbid the exchange of flavon fields eliminating unwanted terms [20–25, 126–128]. In what follows, we will call the whole framework the Flavor-Scoto-Seesaw (FSS) model where each element of the FSS model’s construction is well motivated towards understanding a common origin of θ_{13} and DM. As we employ the A_4 discrete symmetry, compared to Ref. [109] and the Z_8 choice, we have a fuller symmetry with larger particle content. This is the price we pay to predict the TM_2 structure of neutrino masses and mixing. The role of each of Z_N auxiliary symmetries will be explained in detail as we proceed. Interestingly, the model contains an intrinsic Z_2 symmetry under which both f and η are odd. The stability of the dark matter is ensured by this Z_2 symmetry. In Table 1, we present transformation properties of all the fields content of our model under the complete discrete A_4 flavor symmetry. The desired mass matrix structure will be obtained when the flavons get a vacuum expectation value (VEV) in a suitable direction. The VEV alignment considered here is widely used [35, 41, 107] and can be realized in a natural way by analyzing the complete scalar potential [20, 74, 107, 129, 130]. Here, the low energy scalar potential is identical to the potential presented in [102], and for brevity we omit it here. With the fields content of Table 1, the charged lepton Lagrangian can be described by

$$\mathcal{L}_l = \frac{y_e}{\Lambda} (\bar{L}\phi_T) H e_R + \frac{y_\mu}{\Lambda} (\bar{L}\phi_T) H \mu_R + \frac{y_\tau}{\Lambda} (\bar{L}\phi_T) H \tau_R + h.c., \quad (3.1)$$

Fields	e_R, μ_R, τ_R	L_α	H	N_{R_1}	N_{R_2}	f	η	ϕ_s	ϕ_a	ϕ_T	ξ
A_4	$1, 1'', 1'$	3	1	1	1	1	1	3	3	3	$1''$
Z_4	$-i$	$-i$	1	-1	1	1	1	i	$-i$	1	-1
Z_3	ω	ω	ω^2	1	1	1	ω^2	1	1	ω	1
Z_2	-1	1	1	1	-1	-1	1	1	-1	-1	-1

Table 1. Field contents and transformation under the symmetries of our model. The second right-handed neutrino and the flavons field in second block of the table are introduced to implement the A_4 symmetry.

to the leading order, where Λ is the cut-off scale of our model and y_e, y_μ and y_τ are coupling constants. As the SM lepton doublet, L transforms as a triplet under A_4 , the involvement of another triplet is essential as seen in the above Lagrangian. Terms in the first parenthesis of Eq. (3.1) represent the product of two A_4 triplets which results a true singlet after contracting with A_4 singlets e_R, μ_R and τ_R (charged as $1, 1''$ and $1'$ respectively). The multiplication rule of A_4 symmetry is summarized in the Appendix and a detailed discussion on A_4 symmetry can be found in [19, 20]. Now, when the flavon ϕ_T gets VEV in the direction $\langle \phi_T \rangle = (v_T, 0, 0)^T$ [41] and also the Higgs field gets VEV $\langle H \rangle = v$, the charged lepton mass matrix will be a diagonal form

$$M_l = \frac{v_T}{\Lambda} v \begin{pmatrix} y_e & 0 & 0 \\ 0 & y_\mu & 0 \\ 0 & 0 & y_\tau \end{pmatrix}. \quad (3.2)$$

The Lagrangian in the neutrino sector constitutes two parts: a type-I seesaw contribution with two right-handed neutrinos N_{R_1} and N_{R_2} and another is a scotogenic contribution with a scalar field η and a fermionic field f . The Lagrangian that generates neutrino mass at a tree level by the type-I seesaw mechanism in our model can be written as

$$\mathcal{L}_N = \frac{y_{N_1}}{\Lambda} (\bar{L}\phi_s)\tilde{H}N_{R_1} + \frac{y_{N_2}}{\Lambda} (\bar{L}\phi_a)\tilde{H}N_{R_2} + \frac{1}{2}M_{N_1}\bar{N}_{R_1}^c N_{R_1} + \frac{1}{2}M_{N_2}\bar{N}_{R_2}^c N_{R_2} + h.c., \quad (3.3)$$

where $y_{N_{1,2}}$ are the corresponding couplings and $M_{N_{1,2}}$ are the Majorana masses of right-handed neutrinos. To get the flavor structure, we assume that the flavon fields get VEVs along $\langle \phi_s \rangle = (0, v_s, -v_s)$, $\langle \phi_a \rangle = (v_a, v_a, v_a)$ [59, 107]. With these flavon vevs, the Dirac mass matrix will appear from the first two terms of Eq. (3.3) while the Majorana matrix which follows from the next two terms of the Lagrangian of Eq. (3.3) can be found as follows

$$M_D = \frac{v}{\Lambda} \begin{pmatrix} 0 & y_{N_2}v_a \\ -y_{N_1}v_s & y_{N_2}v_a \\ y_{N_1}v_s & y_{N_2}v_a \end{pmatrix} = vY_N, \quad M_R = \begin{pmatrix} M_{N_1} & 0 \\ 0 & M_{N_2} \end{pmatrix}. \quad (3.4)$$

The Z_4 symmetry in Table 1, under which N_{R_1} is odd and N_{R_2} even and the Z_2 symmetry under which N_{R_1} is even and N_{R_2} odd ensures the diagonal structure of M_R as obtained in Eq. 3.4. The

VEV alignment considered here is widely used in the context of form dominance [131], sequential dominance [106], constrained sequential dominance [59] etc., to obtain the textures of the Dirac and Majorana mass matrices. Now using the type-I seesaw formula the light neutrino mass matrix at the leading order can be written as

$$(M_\nu)_{\text{TREE}} = -M_D M_R^{-1} M_D^T. \quad (3.5)$$

With the structure of M_D and M_R obtained in Eq. (3.4), the light neutrino mass matrix is given by

$$(M_\nu)_{\text{TREE}} = - \begin{pmatrix} B & B & B \\ B & A+B & -A+B \\ B & -A+B & A+B \end{pmatrix}, \quad A = \frac{v^2 v_s^2 y_{N_1}^2}{\Lambda^2 M_{N_1}}, \quad B = \frac{v^2 v_a^2 y_{N_2}^2}{\Lambda^2 M_{N_2}}. \quad (3.6)$$

The above mass matrix for light neutrinos obtained from type-I seesaw is incapable to generate non-zero θ_{13} (charged lepton mass matrix being diagonal). As neutrino oscillation data established adequately large θ_{13} , we include a scotogenic contribution to our model to explain correct neutrino mixing which also naturally incorporates few potential DM candidates. The scotogenic contribution in our model with the fermion f and scalar field η can be written as

$$\mathcal{L}_S = \frac{y_s}{\Lambda^2} (\bar{L} \phi_s) \xi i \sigma_2 \eta^* f + \frac{1}{2} M_f \bar{f}^c f + h.c., \quad (3.7)$$

where y_s is the coupling and M_f is the mass of f . Owing to the considered symmetry in Table 1, the leading order contribution $\bar{L} i \sigma_2 \eta^* f$ is disallowed, as it is not invariant under A_4 (and Z_4, Z_2) symmetry. The SM lepton doublet being a triplet under A_4 , just like charged lepton sector, involvement of another A_4 triplet (here ϕ_s) is essential. As a consequence of $Z_{4,2}$ symmetry involvement of the A_4 flavons ϕ_s and ξ is necessary in the first term of Eq. (3.7). The VEV of ϕ_s (mentioned below) and the non-trivial A_4 singlet ξ (provides appropriate A_4 contraction) crucially dictates the structure of the scotogenic contribution and helps in breaking of TBM mixing [71, 74, 92, 132, 133]. Therefore the contribution in the effective neutrino mass matrix originated from the scotogenic radiative corrections is given by [96, 102, 109]

$$(M_\nu)_{\text{LOOP}} = \mathcal{F}(m_{\eta_R}, m_{\eta_I}, M_f) M_f Y_f^i Y_f^j. \quad (3.8)$$

Once the flavons ϕ_s and ξ acquire VEVs in the direction $\langle \phi_s \rangle = (0, v_s, -v_s)$ and $\langle \xi \rangle = v_\xi$ respectively the associated couplings can be written as

$$Y_F = (Y_F^e, Y_F^\mu, Y_F^\tau)^T = (y_s \frac{v_s}{\Lambda} \frac{v_\xi}{\Lambda}, 0, -y_s \frac{v_s}{\Lambda} \frac{v_\xi}{\Lambda})^T. \quad (3.9)$$

Therefore, the corresponding mass matrix takes the form

$$(M_\nu)_{\text{LOOP}} = C \begin{pmatrix} 1 & 0 & -1 \\ 0 & 0 & 0 \\ -1 & 0 & 1 \end{pmatrix}, \quad C = \mathcal{F}(m_{\eta_R}, m_{\eta_I}, M_f) y_s^2 \frac{v_s^2 v_\xi^2}{\Lambda^4}. \quad (3.10)$$

Here $\mathcal{F}(m_{\eta_R}, m_{\eta_I}, M_f)$ is the loop function given in Eq. (2.3). Finally, combining the seesaw and scotogenic contributions, the effective light neutrino mass matrix is the addition of the two mass matrices given in Eq. (3.6) and Eq. (3.10) and reads

$$\begin{aligned}
M_\nu &= (M_\nu)_{\text{TREE}} + (M_\nu)_{\text{LOOP}} \\
&= \begin{pmatrix} -B + C & -B & -B - C \\ -B & -(A + B) & A - B \\ -B - C & A - B & -A - B + C \end{pmatrix}.
\end{aligned} \tag{3.11}$$

In the present context, neutrino masses are obtained through a combination of the type-I seesaw and scotogenic mechanisms. Now, there could also be operators like $LHLH/\Lambda$, which can also contribute to the light neutrino mass. In our model, this term is not invariant under the Z_4 symmetry mentioned in Table 1. Any contributions coming from $LHLH(\phi_a, \phi_s, \phi_T, \xi)/\Lambda^2$ is also disallowed due to the considered discrete symmetries Z_4, Z_3 and Z_2 . For the scotogenic contribution, the coupling $\bar{L}i\sigma_2\eta^*f$ is allowed only at $1/\Lambda^2$ level with the involvement of the flavons ϕ_s, ξ , see Eq. (3.7). In this sector, any higher-order contributions in the bare mass term of f can be absorbed in the leading order contribution. On the other hand for charged lepton sector, the leading contribution only appears at dimension-5 due to the considered A_4 symmetry. There are next-to-leading order corrections present in this sector coming from $(\bar{L}\phi_s\phi_a)H\alpha_R/\Lambda^2$, where α_R is the associated right-handed charged lepton. Thanks to the VEV alignment of the flavons ϕ_s and ϕ_a this term essentially vanishes following the A_4 multiplication rules mentioned in the appendix. For right-handed Majorana neutrinos, the non-vanishing next-to-leading order corrections up-to $\mathcal{O}(1/\Lambda^2)$ in the mass matrix arise from the following terms:

$$\begin{aligned}
\delta\mathcal{L}_{M_R} &= \frac{1}{\Lambda} (\bar{N}_{R_1}^c N_{R_1} + \bar{N}_{R_2}^c N_{R_2}) (\phi_a^\dagger\phi_a + \phi_s^\dagger\phi_s) \\
&+ \frac{1}{\Lambda} (\bar{N}_{R_1}^c N_{R_2} + \bar{N}_{R_2}^c N_{R_1}) (\phi_s^\dagger\phi_a + \phi_s\phi_a^\dagger + \phi_s^\dagger\phi_a^\dagger) + \frac{1}{\Lambda^2} (\bar{N}_{R_1}^c N_{R_2} + \bar{N}_{R_2}^c N_{R_1}) \xi^3.
\end{aligned} \tag{3.12}$$

Here in Eq. (3.12), the first term represents a correction to the diagonal entry which can be absorbed in the leading order M_R . The second term represents off-diagonal entries of the right-handed neutrino mass matrix at $\mathcal{O}(1/\Lambda)$ which also vanishes due to the specific VEV direction of ϕ_s and ϕ_a . The last term in Eq. (3.12) represents off-diagonal entries at $\mathcal{O}(1/\Lambda^2)$. Although this contribution is very small compared to the leading order contribution, it can also be forbidden by considering another Z'_2 symmetry under which charged leptons, f and the flavons ϕ_T, ξ' are odd (while all other particles are even). The Dirac Yukawa coupling is allowed at dimension-5 as given in Eq. (3.3). Here the next-to-leading order contribution at $\mathcal{O}(1/\Lambda)$ can be written as $(\bar{L}\phi_a^\dagger\phi_T)\tilde{H}N_{R_1}/\Lambda^2$ and $(\bar{L}\phi_s^\dagger\phi_T)\tilde{H}N_{R_2}/\Lambda^2$ respectively. These terms are however forbidden owing to the Z_3 symmetry mentioned in Table 1. Therefore, from Table 1, it is clear that along with the A_4 symmetry the auxiliary discrete symmetries crucially dictate allowed structures of the fermionic

mass matrices, and such symmetries are an integral part of the flavor symmetric approach to understand neutrino mixing [20, 37, 40, 41, 134–136].

4 Neutrino masses and mixing in the FSS model

From the previous discussion, we find that the effective neutrino mass matrix consists of two parts, one of them is coming from the type-I seesaw mechanism given by Eq. (3.6) and another one originates from the scotogenic contribution given by Eq. (3.10). Now the mass matrix originating from type-I seesaw given in Eq. (3.6) can be diagonalized by the TBM mixing matrix (U_{TB}) via

$$U_{TB}^T (M_\nu)_{\text{TREE}} U_{TB} = \begin{pmatrix} 0 & 0 & 0 \\ 0 & -3B & 0 \\ 0 & 0 & -2A \end{pmatrix}, \quad (4.1)$$

where

$$U_{TB} = \begin{pmatrix} \sqrt{\frac{2}{3}} & \frac{1}{\sqrt{3}} & 0 \\ -\frac{1}{\sqrt{6}} & \frac{1}{\sqrt{3}} & -\frac{1}{\sqrt{2}} \\ -\frac{1}{\sqrt{6}} & \frac{1}{\sqrt{3}} & \frac{1}{\sqrt{2}} \end{pmatrix}. \quad (4.2)$$

Clearly, a pure type-I seesaw contribution in the present set-up predicts $\theta_{13} = 0$. However, thanks to the scotogenic contribution, we can obtain a deviation from $\theta_{13} = 0$ to be consistent with the observed experimental value [43–45]. Therefore considering the effective light neutrino mass matrix given in Eq. (3.11) and rotating it by U_{TB} , M_ν takes the form

$$\begin{aligned} M'_\nu &= U_{TB}^T M_\nu U_{TB} \\ &= \frac{1}{2} \begin{pmatrix} 3C & 0 & -\sqrt{3}C \\ 0 & -6B & 0 \\ -\sqrt{3}C & 0 & -4A + C \end{pmatrix}, \end{aligned} \quad (4.3)$$

Here we find that the mass matrix in the tri-bimaximal basis is block diagonalized. Therefore a further rotation by a unitary matrix U_{13} in the 13 plane via $M_\nu^{diag} = U_{13}^T M'_\nu U_{13}$ takes M'_ν to a diagonal one. This unitary matrix U_{13} can be parametrized as

$$U_{13} = \begin{pmatrix} \cos \theta & 0 & \sin \theta e^{-i\phi} \\ 0 & 1 & 0 \\ -\sin \theta e^{i\phi} & 0 & \cos \theta \end{pmatrix}, \quad (4.4)$$

where θ is the rotation angle and ϕ is the associated phase factor. The full diagonalization relation of the mass matrix M_ν can be written as

$$(U_{TB} U_{13})^T M_\nu U_{13} U_{TB} = \text{diag}(m_1 e^{i\gamma_1}, m_2 e^{i\gamma_2}, m_3 e^{i\gamma_3}), \quad (4.5)$$

where m_1, m_2, m_3 are the real and positive mass eigenvalues and γ_1, γ_2 and γ_3 are the phases extracted from the corresponding complex eigenvalues. We are now in a position to evaluate the neutrino mixing matrix U_ν such that $U_\nu^T M_\nu U_\nu = \text{diag}(m_1, m_2, m_3)$. Thus U_ν becomes $U_\nu = U_{TB} U_{13} U_m$, where $U_m = \text{diag}(1, e^{i\alpha_{21}/2}, e^{i\alpha_{31}/2})$ is the Majorana phase matrix with $\alpha_{21} = \gamma_1 - \gamma_2$ and $\alpha_{31} = \gamma_1 - \gamma_3$, one common phase being irrelevant. Using Eq. (4.2) and Eq. (4.4), the U_ν mixing matrix in its explicit form can be written as

$$U_\nu = \begin{pmatrix} \sqrt{\frac{2}{3}} \cos \theta & \frac{1}{\sqrt{3}} & \sqrt{\frac{2}{3}} e^{i\phi} \sin \theta \\ -\frac{\cos \theta}{\sqrt{6}} + \frac{e^{i\phi} \sin \theta}{\sqrt{2}} & \frac{1}{\sqrt{3}} & -\frac{\cos \theta}{\sqrt{2}} - \frac{e^{i\phi} \sin \theta}{\sqrt{6}} \\ -\frac{\cos \theta}{\sqrt{6}} - \frac{e^{i\phi} \sin \theta}{\sqrt{2}} & \frac{1}{\sqrt{3}} & \frac{\cos \theta}{\sqrt{2}} - \frac{e^{i\phi} \sin \theta}{\sqrt{6}} \end{pmatrix} U_m. \quad (4.6)$$

Such deviation from the TBM mixing is well known and this particular pattern of U_ν is called TM₂ mixing as described earlier. This lepton mixing matrix U_ν can now be compared with U_{PMNS} which in its standard parametrization is given by [137]

$$U_{PMNS} = \begin{pmatrix} c_{12}c_{13} & s_{12}c_{13} & s_{13}e^{-i\delta_{CP}} \\ -s_{12}c_{23} - c_{12}s_{23}s_{13}e^{i\delta_{CP}} & c_{12}c_{23} - s_{12}s_{23}s_{13}e^{i\delta_{CP}} & s_{23}c_{13} \\ s_{12}s_{23} - c_{12}c_{23}s_{13}e^{i\delta_{CP}} & -c_{12}s_{23} - s_{12}c_{23}s_{13}e^{i\delta_{CP}} & c_{23}c_{13} \end{pmatrix} U_m, \quad (4.7)$$

where θ_{12}, θ_{13} and θ_{23} are three mixing angles, δ_{CP} is the CP violating Dirac phase and α_{21}, α_{31} are the Majorana phases.

The parameters A, B and C appearing in Eq. (4.3) are in general complex, and without loss of generality we can write $A = |A|e^{i\phi_A}$, $B = |B|e^{i\phi_B}$, $C = |C|e^{i\phi_C}$. Now, for calculation purpose, let us define $\alpha = |A|/|C|$ and $\beta = |B|/|C|$, and phase differences $\phi_{AC} = \phi_A - \phi_C$ and $\phi_{BC} = \phi_B - \phi_C$. As U_{13} diagonalizes M'_ν of Eq. (4.3), θ and ϕ can be expressed in terms of model parameters as

$$\tan \phi = \frac{\alpha \sin \phi_{AC}}{1 - \alpha \cos \phi_{AC}}, \quad \tan 2\theta = \frac{\sqrt{3}}{\cos \phi + 2\alpha \cos(\phi_{AC} + \phi)}. \quad (4.8)$$

Further comparing $U_\nu = U_{TB} U_{13} U_m$ as given in Eq. (4.6) with U_{PMNS} as in Eq. (4.7), we find the following relations for mixing angles and δ_{CP} as a function of θ and ϕ as [92, 138–141]

$$\sin \theta_{13} e^{-i\delta_{CP}} = \sqrt{\frac{2}{3}} e^{-i\phi} \sin \theta, \quad \tan^2 \theta_{12} = \frac{1}{2 - 3 \sin^2 \theta_{13}}, \quad (4.9)$$

$$\tan^2 \theta_{23} = \frac{\left(1 + \frac{\sin \theta_{13} \cos \phi}{\sqrt{2 - 3 \sin^2 \theta_{13}}}\right)^2 + \frac{\sin^2 \theta_{13} \sin^2 \phi}{(2 - 3 \sin^2 \theta_{13})}}{\left(1 - \frac{\sin \theta_{13} \cos \phi}{\sqrt{2 - 3 \sin^2 \theta_{13}}}\right)^2 + \frac{\sin^2 \theta_{13} \sin^2 \phi}{(2 - 3 \sin^2 \theta_{13})}}. \quad (4.10)$$

The above relations show that the mixing angles are correlated which is a characteristic feature of the considered A_4 discrete flavor symmetry. For $\sin \theta > 0$, the relation of δ_{CP} implies that $\delta_{CP} = \phi$ and for $\sin \theta < 0$, the same relation implies that $\delta_{CP} = \phi \pm \pi$. Hence, for both cases, we have $\tan \delta_{CP} = \tan \phi$. Now, using Eq. (3.11), the complex mass eigenvalues are calculated to be

$$m_{1,3}^c = -A + C \pm \sqrt{A^2 + AC + C^2}, \quad (4.11)$$

$$m_2^c = -3B. \quad (4.12)$$

The real and positive eigenvalues can be written as

$$m_1 = |C|[(1 - \alpha \cos \phi_{AC} - P)^2 + (Q + \alpha \sin \phi_{AC})^2]^{1/2}, \quad (4.13)$$

$$m_2 = |C|3\beta, \quad (4.14)$$

$$m_3 = |C|[(1 - \alpha \cos \phi_{AC} + P)^2 + (Q - \alpha \sin \phi_{AC})^2]^{1/2}, \quad (4.15)$$

where

$$P^2 = \frac{M \pm \sqrt{M^2 + N^2}}{2}, \quad Q^2 = \frac{-M \pm \sqrt{M^2 + N^2}}{2}, \quad (4.16)$$

$$M = 1 + \alpha \cos \phi_{AC} + \alpha^2 \cos 2\phi_{AC}, \quad N = \alpha \sin \phi_{AC} + \alpha^2 \sin 2\phi_{AC}. \quad (4.17)$$

Following Eq. (4.11) and Eq. (4.12), the phase associated with complex mass eigenvalues $m_{1,2,3}^c$ can be written as $\gamma_i = \phi_C + \phi_i$, where ϕ_i are

$$\phi_1 = \tan^{-1} \left(\frac{Q + \alpha \sin \phi_{AC}}{1 - \alpha \cos \phi_{AC} - P} \right), \quad \phi_2 = \phi_{BC}, \quad \phi_3 = \tan^{-1} \left(\frac{Q - \alpha \sin \phi_{AC}}{1 - \alpha \cos \phi_{AC} + P} \right). \quad (4.18)$$

The two Majorana phases in U_m (see eq. (4.6)) therefore can be derived as

$$\alpha_{21} = \tan^{-1} \left(\frac{Q + \alpha \sin \phi_{AC}}{1 - \alpha \cos \phi_{AC} - P} \right) - \phi_{BC}, \quad (4.19)$$

$$\alpha_{31} = \tan^{-1} \left(\frac{Q + \alpha \sin \phi_{AC}}{1 - \alpha \cos \phi_{AC} - P} \right) - \tan^{-1} \left(\frac{Q - \alpha \sin \phi_{AC}}{1 - \alpha \cos \phi_{AC} + P} \right). \quad (4.20)$$

The overall phase factor ϕ_C appearing in γ_i has no physical significance in computing the Majorana phases. The mixing angles and the phases depend on the parameters $\alpha, \phi_{AC}, \phi_{BC}$ whereas the light neutrino masses depend on these parameters as well as on β and $|C|$ as observed in Eq. (4.8) - Eq. (4.20). In the next section, we constrain these parameters using experimental data for neutrino mixing angles and masses.

parameters	best-fit	3σ range
$\frac{\Delta m_{21}^2}{10^{-5} \text{eV}^2}$	7.50	6.94 - 8.14
$\frac{ \Delta m_{31}^2 }{10^{-3} \text{eV}^2} (\text{NH})$	2.55	2.47 - 2.63
$\frac{ \Delta m_{31}^2 }{10^{-3} \text{eV}^2} (\text{IH})$	2.45	2.37 - 2.53
$\sin^2 \theta_{12}/10^{-1}$	3.18	2.71 - 3.69
$\sin^2 \theta_{13}/10^{-2} (\text{NH})$	2.200	2.000 - 2.405
$\sin^2 \theta_{13}/10^{-2} (\text{IH})$	2.225	2.018 - 2.424
$\sin^2 \theta_{23}/10^{-1} (\text{NH})$	5.74	4.34 - 6.10
$\sin^2 \theta_{23}/10^{-1} (\text{IH})$	5.78	4.33 - 6.08

Table 2. Global fits of three active-neutrino oscillation data taken for Ref. [5] for NH and IH, used in our analysis.

5 Numerical analysis of the FSS model

In order to constrain the parameters involved in our analysis, using Eq. (4.13) - Eq. (4.15), we can define a ratio r as

$$r = \frac{\Delta m_{21}^2}{|\Delta m_{31}^2|}, \quad (5.1)$$

where $\Delta m_{21}^2 = m_2^2 - m_1^2$ and $|\Delta m_{31}^2| = |m_3^2 - m_1^2|$ are the solar and atmospheric mass squared differences. From the expressions for the mixing angles (namely, θ_{13} , θ_{12} and θ_{23}) as well as the absolute neutrino masses ($m_{1,2,3}$), their sum ($\sum m_i$) and the ratio r defined in Eq. (5.1) all depend on the variables α , β , ϕ_{AC} and ϕ_{BC} as discussed in Section 4. Over the last two decades neutrino oscillation parameters have been measured with incredible accuracy [5, 142, 143]. Therefore using the precisely determined neutrino oscillation data on θ_{13} , θ_{12} , θ_{23} , r , Δm_{21}^2 and $|\Delta m_{31}^2|$ one can constrain four model parameters. Once the model parameters are constrained, we can further compute the Dirac CP phase δ_{CP} , Majorana phases α_{21} , α_{31} , the sum of the absolute masses of the three light neutrinos ($\sum m_i$) as well as the effective mass parameter appearing in the neutrinoless double beta decay ($m_{\beta\beta}$). Table 2 summarizes the best fit and 3σ ranges of the neutrino oscillation data [5] for both normal and inverted hierarchy of light neutrino masses which are used in the subsequent numerical analysis.

Before we proceed further, let us point out that the correlation between the mixing angles θ_{13} and θ_{12} given in Eq. (4.9) is a feature of the TM_2 mixing mentioned above [139, 141]. In Fig. 1, we have plotted this $\sin^2 \theta_{12} - \sin^2 \theta_{13}$ correlation for TM_2 mixing and we find that $\sin^2 \theta_{12}$ is restricted

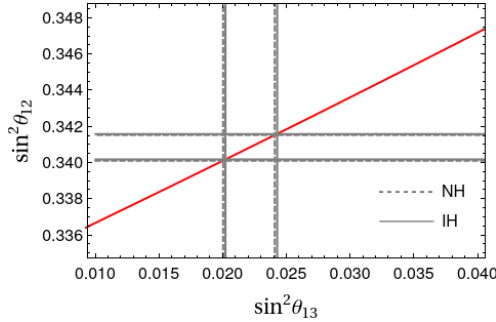


Figure 1. $\sin^2 \theta_{12}$ is plotted against $\sin^2 \theta_{13}$ for both NH and IH of neutrino masses. The vertical grid-lines are 3σ allowed for $\sin^2 \theta_{13}$ and horizontal grid-lines represent corresponding restriction on $\sin^2 \theta_{12}$ in our analysis.

within a narrow range (between $0.3401 \leq \sin^2 \theta_{12} \leq 0.3415$) corresponding to the 3σ ranges of $\sin^2 \theta_{13}$. Now, in order to evaluate absolute neutrino masses we also need to find the overall factor $|C|$ appearing in the mass eigenvalues given in Eq. (4.13) - Eq. (4.15). Although this common factor $|C|$ cancels out when we calculate r but $|C|$ can be calculated by fitting the solar (or atmospheric)

mass-squared differences knowing the model parameters. After $|C|$ is evaluated, we can get the estimation of absolute neutrino masses $m_{1,2,3}$ and their sum $\sum m_i$. Similarly, substituting the estimations for α, β, ϕ_{AC} and ϕ_{BC} in Eq. (4.19) and Eq. (4.20) we can also quantify the Majorana phases. Knowing the neutrino mixing angles, masses, and associated CP phases, finally in our analysis, we will have a prediction on the effective neutrino mass parameter $m_{\beta\beta}$ characterizing the neutrinoless double beta decay. The effective mass parameter $m_{\beta\beta}$ can be described as a function of the lightest neutrino mass (m_1 for NH and m_3 for IH respectively) and can be written as ²

$$\text{NH: } m_{\beta\beta} = \left| m_1 c_{12}^2 c_{13}^2 + \sqrt{m_1^2 + \Delta m_{21}^2} s_{12}^2 c_{13}^2 e^{i\alpha_{21}} + \sqrt{m_1^2 + \Delta m_{31}^2} s_{13}^2 e^{i(\alpha_{31} - 2\delta_{\text{CP}})} \right|, \quad (5.2)$$

$$\text{IH: } m_{\beta\beta} = \left| \sqrt{m_3^2 + \Delta m_{31}^2} c_{12}^2 c_{13}^2 + \sqrt{m_3^2 + \Delta m_{31}^2 + \Delta m_{21}^2} s_{12}^2 c_{13}^2 e^{i\alpha_{21}} + m_3 s_{13}^2 e^{i(\alpha_{31} - 2\delta_{\text{CP}})} \right| \quad (5.3)$$

Now, for a better understanding of the behaviour of the parameters involved and the model predictions, we can divide our numerical analysis into some special cases by taking some particular values of the relative phases ϕ_{AC} and ϕ_{BC} . All mixing angles in Eq. (4.9), (4.10) and neutrino mass eigenvalues in Eq. (4.13) - Eq. (4.15) and the Majorana phase α_{31} depend on one relative phase, namely, ϕ_{AC} . In contrast, the other Majorana phase α_{21} as well as $m_{\beta\beta}$ depend on both ϕ_{AC} and ϕ_{BC} . In the following, we choose five simple special cases depending on the values of these phases, namely: (i) Case I : $\phi_{AC} = 0, \phi_{BC} = 0$, (ii) Case II $\phi_{AC} = 0$, (iii) Case III $\phi_{AC} = \phi_{BC}$, (iv) Case IV $\phi_{BC} = 0$ and subsequently in (v) Case V we present the general scenario where both ϕ_{AC} and ϕ_{BC} vary between $0 - 2\pi$. Below, we have explored these cases and as we proceed it will be clear that some of these cases have the potential to distinguish the normal and inverted hierarchy of light neutrino masses and produce interesting predictions on neutrino parameters.

5.1 Case I: $\phi_{AC} = \phi_{BC} = 0$

Here we make the simplest choice for the relative phases, *i.e.*, $\phi_{AC} = \phi_{BC} = 0$. With this value, the Eq. (4.8) and (4.9) have the simple form

$$\tan 2\theta = \frac{\sqrt{3}}{1 + 2\alpha}, \quad \sin \theta_{13} = \sqrt{\frac{2}{3}} |\sin \theta|. \quad (5.4)$$

with $\tan \delta_{\text{CP}} = 0$. Clearly, $\sin \theta_{13}$ only depends on α and in Fig. (2) left panel, we have plotted $\sin \theta_{13}$ as a function of α using Eq. (5.4). The 3σ allowed range for $\sin \theta_{13}$ (given by the area between horizontal lines) restricts α within 1.6465 – 1.8754 (1.6557 – 1.8391) for IH (NH) given by the dashed (continuous) vertical lines. With $\phi_{AC} = \phi_{BC} = 0$ the real positive mass eigenvalues

²The expression for the effective mass parameter $m_{\beta\beta}$ can also be written in a symmetrical form where only two Majorana phases [144] appear instead of three phases appearing in the standard PDG parametrization [145].

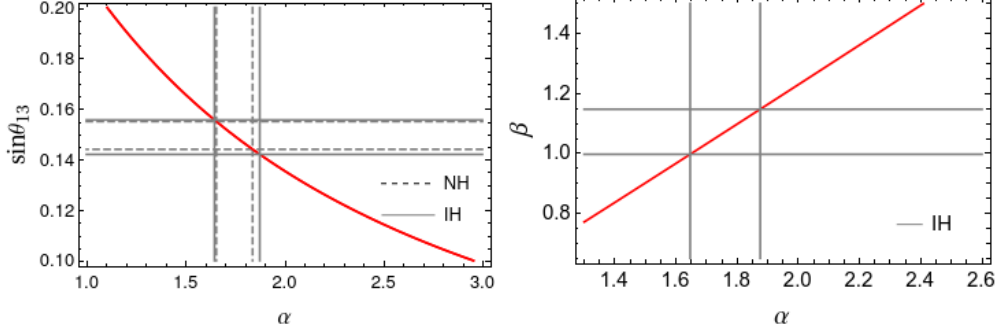


Figure 2. Left Panel: Plot for $\sin\theta_{13}$ vs α . Horizontal grid lines are the 3σ allowed range for $\sin\theta_{13}$ (for NH and IH) whereas the vertical grid lines represent the corresponding allowed range for α (1.6557 – 1.8391 and 1.6465 – 1.8754 for NH and IH respectively). Right Panel: Contour plot for $r = 0.03$ in $\alpha - \beta$ plane. The vertical grid lines represent the allowed regions for α from the left panel and the horizontal grid lines are the corresponding allowed regions for β .

given in Eq. (4.13) - Eq. (4.15) can be expressed as

$$m_1 = |C|(1 - \alpha - \sqrt{1 + \alpha + \alpha^2}), \quad (5.5)$$

$$m_2 = |C|3\beta, \quad (5.6)$$

$$m_3 = |C|(1 - \alpha + \sqrt{1 + \alpha + \alpha^2}). \quad (5.7)$$

With the above mass eigenvalues, one can write the ratio of solar to atmospheric mass-squared differences as defined in Eq. (5.1) as

$$r = \pm \frac{9\beta^2 - (1 - \alpha - \sqrt{1 + \alpha + \alpha^2})^2}{(1 - \alpha + \sqrt{1 + \alpha + \alpha^2})^2 - (1 - \alpha - \sqrt{1 + \alpha + \alpha^2})^2}, \quad (5.8)$$

where the \pm signs are for NH and IH respectively. When $\phi_{AC} = \phi_{BC} = 0$, as a consequence of the considered discrete flavor symmetry, NH of light neutrino masses can not be realized with Eq. (5.5) - Eq. (5.8). Hence only IH of light neutrino masses is allowed. From Eq. (5.8), we notice that r depends on both α and β and in the right panel of Fig. 2, we have plotted this dependence in this $\alpha - \beta$ plane for the best fit value of the ratio r ($= 0.03$) [5] only for IH. For the 3σ allowed range for α (fitting $\sin\theta_{13}$), obtained from the left panel of Fig. 2, β found to be in the range 0.997 – 1.14 for IH. The contour plot for r yields a one-to-one correspondence between α and β as evident from the right panel of Fig. 2. For example, the best fit value of $\sin\theta_{13}$ and r fixes $\alpha : 1.752, \beta : 1.067$ for IH. With the known sets of (α, β) corresponding to 3σ range of $\sin\theta_{13}$, we can calculate $|C|$ by fitting the best fit value of the solar mass-squared difference (given in Table 2) as $|C| = (2.04 - 1.68) \times 10^{-2}$ eV. Then, for the allowed sets of $(\alpha, \beta, |C|)$, we can estimate the absolute neutrino masses $m_{1,2,3}$ and their sum $\sum m_i$. In Fig. 3, we have plotted the individual neutrino masses $m_{1,2,3}$ (by blue dashed, red and orange lines respectively) and their sum $\sum m_i$ (green line) against α as obtained

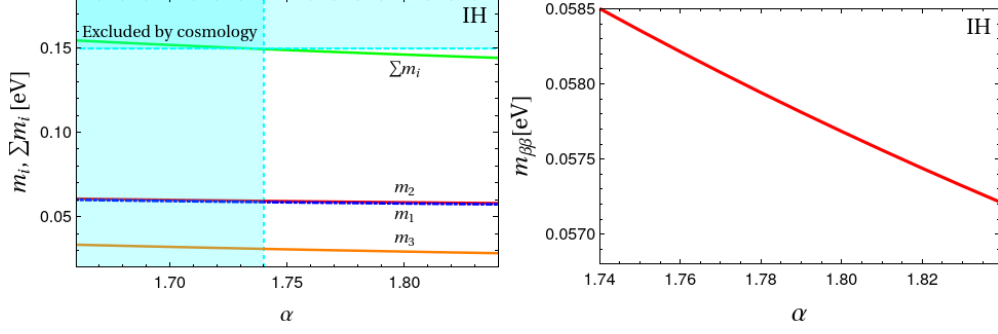


Figure 3. Left Panel: Absolute neutrino masses m_3 (orange line), m_2 (blue dashed line), m_3 (red line) and their sum $\sum m_i$ (green line) plotted against α . Right Panel : The prediction on the effective mass parameter $m_{\beta\beta}$. In both cases we have considered $\phi_{AC} = \phi_{BC} = 0$.

from the left panel of Fig. 2. Now for IH, cosmology sets an upper limit on the sum of the masses of three light neutrinos as $\sum m_i \leq 0.15$ eV [5] as given by the horizontal cyan shaded region in the left panel of Fig. 3. Thus all (α, β) found from the the right panel of Fig. 2 are not allowed. The vertical dashed line in the left panel of Fig. 3 thus represents a further restriction on α (and hence on β) and the lower bound on α shifted from 1.6567 to 1.74. As a result the corresponding values of β and $|C|$ will also be shifted. The final allowed values of the model parameters are summarized in Table. 3. Substituting $\phi_{AC} = 0$ in Eq. (4.18) we obtain $\phi_1 = \phi_3 = 0$ and with $\phi_{BC} = 0$ we

Parameters	Allowed ranges
α	1.74-1.875
β	1.059-1.147
$ C $ (eV)	$(1.87-1.68) \times 10^{-2}$
$\sum m_i$ (eV)	0.1496-0.1408
$m_{\beta\beta}$ (eV)	0.0568-0.0585

Table 3. The allowed ranges for α , β , $|C|$, $\sum m_i$ and $m_{\beta\beta}$ when $\phi_{AC} = \phi_{BC} = 0$.

get $\phi_2 = 0$. Altogether substituting these in Eq. (4.19) and Eq. (4.20), the Majorana phases are found to be zero. Thus for vanishing values of the relative phase $\phi_{AC} = 0$ and $\phi_{BC} = 0$, the Dirac and Majorana phases also vanishes. With these values of the phases and known sets of $(\alpha, \beta, |C|)$ we can now finally estimate the effective mass parameter $m_{\beta\beta}$ appearing in the neutrinoless double beta decay. In the right panel of Fig. 3, we have plotted the prediction for $m_{\beta\beta}$ as a function of α with $\phi_{AC} = \phi_{BC} = 0$. The finding for the sum of the absolute neutrino masses and the effective mass parameter as obtained from Fig. 3 are also summarized in Table 3.

5.2 Case II : $\phi_{AC} = 0$

In the second case, we consider $\phi_{AC} = 0$ but do not make any choice of ϕ_{BC} . We already know that neutrino mixing angles and neutrino masses both depend on the phase ϕ_{AC} alone, which can be understood from the general expressions of Eq. (4.8) - Eq. (4.10) and Eq. (4.13) - Eq. (4.15). The Majorana phases α_{21} and hence neutrinoless double beta decay effective mass parameter $m_{\beta\beta}$ depend on both ϕ_{AC} and ϕ_{BC} . Now, with the choice of $\phi_{AC} = 0$, the simplified expressions for θ and $\sin\theta_{13}$ are same as in Eq. (5.4). The real positive mass eigenvalues and the ratio of the mass-squared differences r will take the form as in Eqs. (5.5) - (5.8) respectively. Hence, with these expressions, the limits on α , β , $|C|$, m_i and Σm_i will same as in Case I ($\phi_{AC} = \phi_{BC} = 0$) which are summarized in Table 3. Thus in this case too only IH of light neutrino masses is allowed. The only difference between Case I and Case II is that in the latter case ϕ_{BC} is free. As ϕ_{BC} only appears for Majorana phases, which can be understood just by looking at the Eq. (4.18), the prediction on Majorana phases will be different from the previous case and hence prediction on $m_{\beta\beta}$ will change accordingly. For $\phi_{AC} = 0$, ϕ_1 and ϕ_3 are zero (obtained from Eq. (4.18)) as mentioned in Case I. Hence, one of the Majorana phase α_{31} vanishes but due to non-zero ϕ_2 , the other Majorana phase (α_{21}) found to be $\alpha_{21} = -\phi_{BC}$. Hence, we will calculate the neutrinoless double beta decay effective mass parameter $m_{\beta\beta}$ using Eq. (5.2) by choosing different values for ϕ_{BC} . In Table 4

ϕ_{BC}	$\pi/6$	$\pi/3$	$\pi/2$	$2\pi/3$	$5\pi/6$	π
$m_{\beta\beta}$ (eV)	0.057-0.055	0.051-0.050	0.043-0.042	0.034-0.033	0.024-0.023	0.019-0.018

Table 4. Prediction on $m_{\beta\beta}$ depending on different values of ϕ_{BC} in the Case II with $\phi_{AC} = 0$.

where we have summarized the ranges of $m_{\beta\beta}$ for different values of ϕ_{BC} such as $\phi_{BC} = \pi/6, \pi/3, \pi/2, 2\pi/3, 5\pi/6$ and π . Prediction on $m_{\beta\beta}$ in this case for $\phi_{BC} = 0 - \pi$ recurs the same value again for $\phi_{BC} = \pi - 2\pi$. From Case I and Case II, one can say that only IH is allowed with $\phi_{AC} = 0$ (with $\phi_{BC} = 0$ or arbitrary).

5.3 Case III: $\phi_{AC} = \phi_{BC} = \phi_x$

In this case, we consider the scenario when the relative phases ϕ_{AC} and ϕ_{BC} both are equal, say, $\phi_{AC} = \phi_{BC} = \phi_x$. Hence, the general expressions for the rotation angle θ and associated phase ϕ appearing in the unitary rotation matrix U_{13} as given in Eq. (4.8) can be rewritten as

$$\tan\phi = \frac{\alpha \sin\phi_x}{1 - \alpha \cos\phi_x}, \quad \tan 2\theta = \frac{\sqrt{3}}{\cos\phi + 2\alpha \cos(\phi_x + \phi)}. \quad (5.9)$$

Thus we can substitute ϕ in the second equation above to evaluate $\sin\theta_{13}$ using Eq. (4.9). Furthermore as $\tan\delta_{CP} = \tan\phi$, we find that a particular value of δ_{CP} , $\sin\theta_{13}$ both depends on ϕ_x and α . In Fig. 4 we provide contour plots for $\sin\theta_{13} = 0.148$ and $\delta_{CP} = 0.541$ (or 31°) denoted by purple and blue dotted lines respectively. The intersection between $\sin\theta_{13}$ and δ_{CP} contours indicate the

simultaneous satisfaction of them and Fig. 4 it is indicated by a black dot with which a pair of $\cos \phi_x$ and α are attached. Similar intersections of the green dot-dashed lines ($\delta_{\text{CP}} \leq 0.541$) with the purple line represent other pairs of $\cos \phi_x$ and α . In this case the mass eigenvalues m_1 , m_2 and

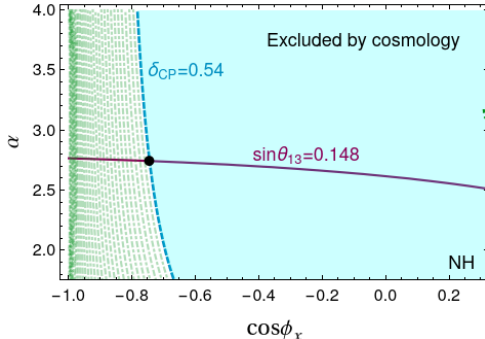


Figure 4. The contour plot for $\delta_{\text{CP}} = 0.78$ (blue dots) and best fit of $\sin \theta_{13}$ (red) for NH of neutrino masses. The region between red dots represents the 3σ region of $\sin \theta_{13}$ value of neutrino oscillation data for NH of neutrino masses. The intersection point represents the value of α and $\cos \phi_x$.

m_3 can be written as

$$m_1 = |C| \left[(1 - \alpha \cos \phi_x - P)^2 + (Q + \alpha \sin \phi_x)^2 \right]^{1/2}, \quad (5.10)$$

$$m_2 = |C| 3\beta, \quad (5.11)$$

$$m_3 = |C| \left[(1 - \alpha \cos \phi_x + P)^2 + (Q - \alpha \sin \phi_x)^2 \right]^{1/2}, \quad (5.12)$$

and using these equations we can also evaluate the ratio of the mass-squared differences r using Eq. (5.1). One can then compute β with $r = 0.03$ and the corresponding value for $|C|$ for each pair of α and $\cos \phi_x$ obtained from intersecting points in Fig. 4. With this flavor structure of the mass eigenvalues given in Eq. (5.10) - Eq. (5.12), the inverted hierarchy of neutrino mass is not possible with $\phi_{AC} = \phi_{BC}$. For each set of α, β, ϕ_x and $|C|$ estimated above, we can predict the sum of the absolute neutrino mass $\sum m_i$ and in Table 5 we present few such representative values. From Eq. (4.18) - Eq. (4.20), we find that the Majorana phases α_{21} and α_{31} are defined as $\alpha_{21} = \phi_1 - \phi_2$ and $\alpha_{31} = \phi_1 - \phi_3$ where ϕ_1, ϕ_2 and ϕ_3 in the present case can be written as

$$\phi_1 = \tan^{-1} \left(\frac{Q + \alpha \sin \phi_x}{1 - \alpha \cos \phi_x - P} \right), \quad \phi_2 = \phi_x, \quad \phi_3 = \tan^{-1} \left(\frac{Q - \alpha \sin \phi_x}{1 - \alpha \cos \phi_x + P} \right). \quad (5.13)$$

Substituting α and $\cos \phi_x$ obtained from Fig. 4 in the above equations we can compute the Majorana phases and estimate the effective mass parameter appearing in the neutrinoless double beta decay as defined in Eq. (5.2). These predictions for $m_{\beta\beta}$ are listed in the last column of Table 5. From the results obtained from Fig. 4 and Table 5, we find that all values for δ_{CP} are not compatible with the cosmological bound on the sum of neutrino masses $\sum m_i$ (satisfying correct neutrino oscillation

δ_{CP}	α	$\cos \phi_x$	β	$ C $ (eV)	$\sum m_i$ (eV)	$m_{\beta\beta}$ (eV)	$m_{\beta\beta} _{\phi_{BC}=0}$ (eV)
0.087	2.765	-0.9848	0.5721	0.0084	0.0773	0.00589	0.0128
0.174	2.765	-0.9659	0.5895	0.00858	0.0792	0.0077	0.0148
0.262	2.765	-0.9327	0.6356	0.008956	0.0804	0.0100	0.0141
0.349	2.759	-0.8853	0.7089	0.0096	0.0922	0.0144	0.0108
0.436	2.754	-0.8332	0.7849	0.0104	0.1026	0.0188	0.0188
0.523	2.754	-0.7669	0.872	0.0117	0.1181	0.0252	0.0259
0.541	2.754	-0.748	0.894	0.0122	0.123	0.0257	0.0251

Table 5. The allowed ranges of parameters satisfying neutrino data for various values of δ_{CP} with $\phi_{AC} = \phi_{BC}$. The last column represents prediction for $m_{\beta\beta}$ for $\phi_{AC} = 0 \div 2\pi$ and $\phi_{BC} = 0$.

data). The region $\delta_{\text{CP}} \leq 0.54$ (31°) given by the cyan shaded region is disallowed due to the cosmological upper bound $\sum m_i \leq 0.12$ eV for NH [5]. Thus the green dot-dashed region in Fig. 4 with $0 < \delta_{\text{CP}} \leq \pi/6$ satisfy both neutrino oscillation data and the cosmological bound on the sum of neutrino masses. In Table 5 we have summarized constraints on α , β , $\cos \phi_x$ and $|C|$ for a specific value of δ_{CP} as well as predictions on $\sum m_i$ and $m_{\beta\beta}$. Here we also find that predictions for the parameters given in Table 5 repeats again for $\pi < \delta_{\text{CP}} \leq 7\pi/6$. From the results summarized in the Table 5 one can find that with increase of $(\beta, \cos \phi_x, |C|)$, α decreases whereas both $\sum m_i$, $m_{\beta\beta}$ increases with the increase of δ_{CP} .

5.4 Case IV: $\phi_{BC} = 0$

In this case we consider $\phi_{BC} = 0$ while ϕ_{AC} is varied arbitrarily between $0 - 2\pi$. This scenario is very similar to the previous case. with $\phi_{AC} = \phi_{BC} = \phi_x$. From Eq. (4.18)–(4.20) we find that $\phi_{BC} = 0$ only effects the Majorana phases and hence the effective mass parameter appearing in the neutrinoless double beta decay. The conclusion drawn in Case III for absolute values of light neutrino masses and their hierarchy will be identical. For simplicity and resembles to the previous case, we consider $\phi_{AC} = \phi_x$. With this, the expressions for rotation angle θ and the phase ϕ appearing in U_{13} are already given in Eq. (5.9). Using Eq. (4.9) we also find that δ_{CP} and $\sin \theta_{13}$ are both function of α and ϕ_x . For a particular value of δ_{CP} we can again compute the pairs of α and ϕ_x from the intersections of contour plots for the chosen value of δ_{CP} and best-fit value of $\sin \theta_{13}$ as given in Fig. 4. Similar to Case III, by fitting $r = 0.03$, we can get β (and subsequently $|C|$), where the expression of r in Eq. (5.1) involves neutrino masses those are given in Eq. (5.10) - Eq. (5.12). Therefore the results of Table 5 will be same for this case up-to the sixth column for $\sum m_i$. The change will occur in the seventh column of Table 5 as here in Case IV, we have $\phi_{BC} = 0$. Although, with this choice, the expression for ϕ_1 and ϕ_3 will be the same as Eq. (5.13) but unlike the previous case we have $\phi_2 = 0$ here. The two Majorana phases follow the relation

$\alpha_{21} = \phi_1 - \phi_2$, $\alpha_{31} = \phi_1 - \phi_3$ hence α_{31} will be identical and α_{21} will be different from Case III. As a result, $m_{\beta\beta}$ will be different compared to the previous scenario. Hence in the last column of Table 5 we append the prediction of $m_{\beta\beta}$ for a few allowed values for δ_{CP} . Note that here also the allowed ranges of the Dirac CP phase are $0 < \delta_{\text{CP}} \leq \pi/6$ and $\pi < \delta_{\text{CP}} \leq 7\pi/6$ respectively which satisfy both neutrino oscillation data and the cosmological bound on the sum of absolute neutrino masses. A point to remember is that this case only satisfies NH of neutrino mass and IH is not allowed.

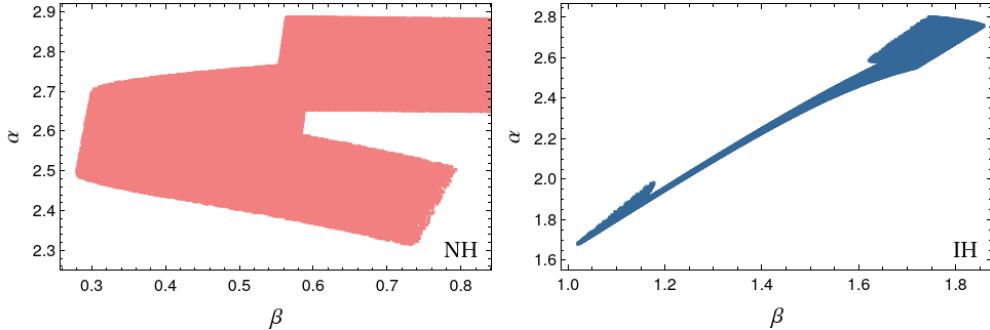


Figure 5. The allowed regions for α and β for the 3σ ranges for $\sin^2 \theta_{13}$ and r for NH (left panel, light red shaded region) and IH (right panel, blue shaded region) of neutrino masses where ϕ_{AC} and ϕ_{BC} are varied from 0 to 2π .

5.5 General case

In the above cases, we have analyzed neutrino mixing for various limiting values for the relative phases associated with our study. Now, we will carry out a full numerical analysis for the most general case where we vary both ϕ_{AC} and ϕ_{BC} to their entire range from 0 to 2π . Then, Eq. (4.8) - Eq. (4.10) will be used for the calculation of mixing angles. On the other hand, the ratio of the mass-squared differences r defined in Eq. (5.1) can also be calculated using the general expression for the mass eigenvalues of Eq. (4.13) - Eq. (4.15). As explained earlier, in order to evaluate the absolute neutrino masses, we also need to evaluate the common factor $|C|$ associated with each mass eigenvalue. Here we obtain $|C|$ by fitting the solar mass-squared difference taken from [5]. In our analysis for this most general case, we have also included the bound coming from cosmological observations on the sum of absolute neutrino masses as $\sum m_i < 0.12$ eV for NH and $\sum m_i < 0.15$ eV for IH [5]. Using the 3σ allowed range for the neutrino oscillation data [5] given in Table 2, we vary both ϕ_{AC} and ϕ_{BC} between 0 to 2π . In Fig. 5 we have plotted the allowed region in the $\alpha - \beta$ plane for NH (left panel, light red shaded region) and IH (right panel, blue shaded region) respectively. Here we find that for NH (IH), the allowed ranges for α vary between $2.33 \leq \alpha \leq 2.9$ ($1.65 \leq \alpha \leq 2.8$). On the other hand, allowed ranges for β are restricted by $0.3 \leq \beta \leq 1$ for

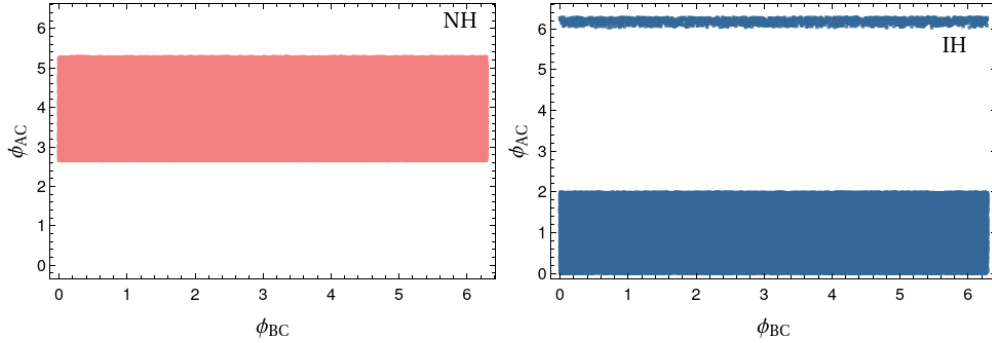


Figure 6. The allowed ranges for ϕ_{AC} and ϕ_{BC} for the correct value of $\sin^2 \theta_{13}$ and r along with for both NH (left panel) and IH (right panel) of neutrino masses.

NH whereas for IH we have $1.9 \geq \beta \geq 1$. This implies β values less than 1 are favored for NH whereas values greater than 1 are favored for IH. Similarly, in Fig. 6 we have plotted the allowed region in $\phi_{AC} - \phi_{BC}$ plane for NH (left panel, light red shaded region) an IH (right panel, blue shaded region) respectively. Here ϕ_{BC} between $0 - 2\pi$ is compatible for both of the hierarchies, however, two distinct regions for ϕ_{AC} are allowed, namely, $2.61 \leq \phi_{AC} \leq 5.38$ for NH and $\phi_{AC} \leq 2$ & $6 \leq \phi_{AC} \leq 2\pi$ for IH respectively. Clearly, the full range of ϕ_{BC} is allowed because it is not sensitive to low energy masses, and mixing and only appears in one of the Majorana phase α_{21} . Thus the values of ϕ_{AC} crucially dictate the hierarchy of light neutrino masses. As an artifact of the considered flavor symmetry, combining the results from Fig. 5 and 6, we can conclude that with $\beta \leq 1$ and $2.61 \leq \phi_{AC} \leq 5.38$ one can reproduce NH whereas to obtain IH we need $\beta \geq 1$ and $0 \leq \phi_{AC} \leq 2$ (or $6 \leq \phi_{AC} \leq 2\pi$).

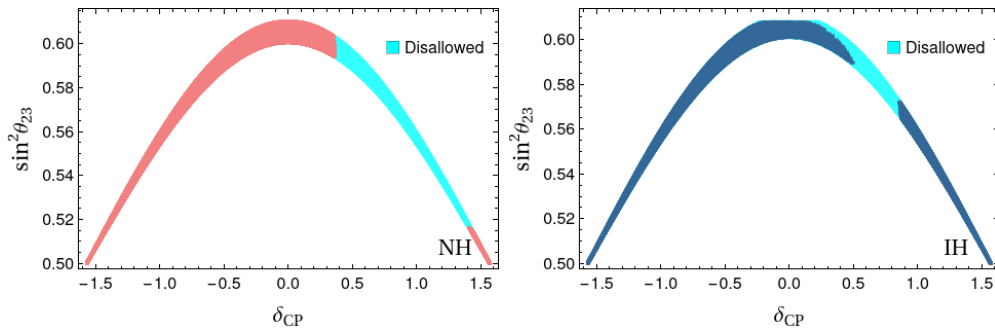


Figure 7. $\sin^2 \theta_{23} - \delta_{CP}$ correlation for NH (left panel) and IH (right panel). The cyan patch represents the disallowed region coming from the constraints on light neutrino masses.

Now with the allowed values for α, β, ϕ_{AC} and ϕ_{BC} obtained from Fig. 5 and 6, we are now equipped to study the correlation between neutrino mixing parameters and predictions associated with the phases and masses. Due to the presence of the A_4 discrete flavor symmetry, this model

yields an interesting correlation among the observables appearing in neutrino mixing. Following Eq. (4.8) - Eq. (4.10), we find one such important correlation between the atmospheric mixing angle θ_{23} and Dirac CP phase δ_{CP} . This correlation is very crucial because still there are some unsettled issues with the measurement of these two oscillation parameters such as (a) octant of θ_{23} , i.e., $\theta_{23} < 45^\circ$ (lower octant, LO) or $\theta_{23} > 45^\circ$ (higher octant, HO) and (b) magnitude of Dirac CP phase δ_{CP} . The $\delta_{\text{CP}} - \theta_{23}$ correlation obtained here is plotted in Fig. 7 and given by light red (blue) shaded region for NH (IH) in the left (right) panel and shades some light on the above mentioned unsettled issues. It is evident from Fig. 7 that for both hierarchies only higher octant of θ_{23} is favoured (i.e. $\theta_{23} \geq 45^\circ$) in our analysis. Furthermore, the cyan patch in both of the panels represents the disallowed region for δ_{CP} in order to satisfy the limits on light neutrino masses [5]. From Fig. 7 the allowed regions for Dirac CP phase δ_{CP} are given by $-1.57 \leq \delta_{\text{CP}} \leq 1.37$ and $1.4 \leq \delta_{\text{CP}} \leq 1.57$ for NH, whereas for IH the predictions are $-1.57 \leq \delta_{\text{CP}} \leq 0.5$ and $0.86 \leq \delta_{\text{CP}} \leq 1.57$. The disallowed region for δ_{CP} is small in IH of neutrino masses compared to the NH as cosmology puts a tighter constraint on NH compared to IH [5].

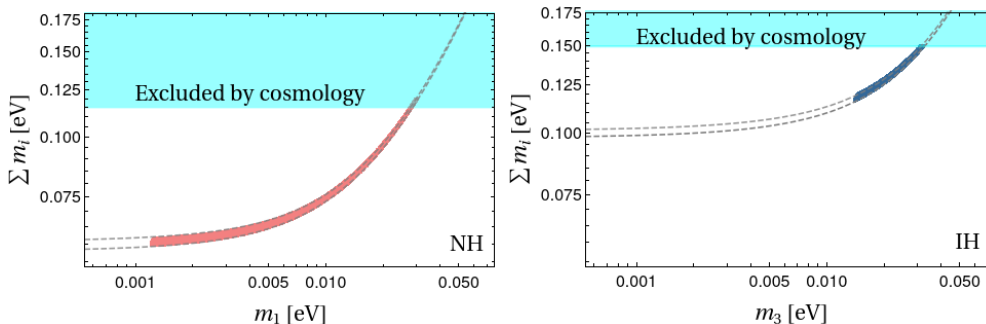


Figure 8. Sum of absolute neutrino masses $\sum m_i$ plotted against lightest neutrino mass for both NH (left panel, light red shaded region) and IH (right panel, blue shaded region). The area between the dashed lines represents 3σ allowed range and the cyan patch represents the area excluded by cosmology.

Again, with the permitted values of α , β , ϕ_{AC} and ϕ_{BC} , we have the predictions on light neutrino masses which can be understood from the correlation plot of $\sum m_i$ vs lightest neutrino (m_1 for NH and m_3 for IH) mass for both hierarchies as given in Fig. 8. Here also the allowed regions are given by light red (blue) shaded region for NH (IH) in the left (right) panel. The horizontal cyan region in each plot represents the disallowed regions mentioned earlier in this subsection. Clearly, this framework predicts that the lightest neutrino mass can take smaller values for NH ($m_{\text{lightest}} \geq 0.0012$ eV), compared to the IH scenario ($m_{\text{lightest}} \geq 0.014$ eV). In Fig. 7, we showed the $\sin^2 \theta_{23} - \delta_{\text{CP}}$ correlation which is generic feature for the TM_2 mixing. Now to elucidate the additional predictions which go beyond TM_2 mixing in FSS, we present a few additional correlations among neutrino masses and mixing. Hence in Fig. 9 we plot the correlation between the sum of

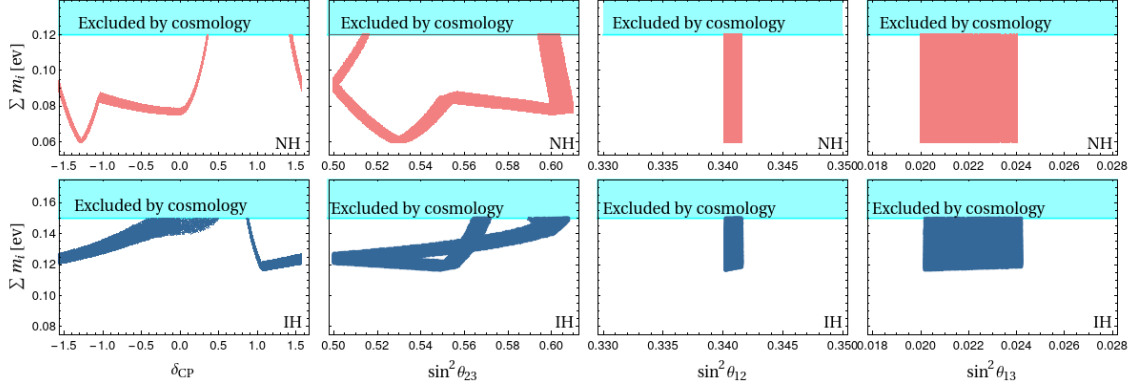


Figure 9. The correlation plot between $\sum m_i$ and δ_{CP} , $\sin^2 \theta_{23}$, $\sin^2 \theta_{12}$, $\sin^2 \theta_{13}$. The upper panels are schematics for NH whereas the lower panel is for IH and the cyan patch represents the area excluded by cosmology.

absolute neutrino masses $\sum m_i$ and other observables such as δ_{CP} , $\sin^2 \theta_{23}$, $\sin^2 \theta_{12}$ and $\sin^2 \theta_{13}$ in the FSS framework. Here the upper panel with light red shaded regions represents the allowed parameter space for NH whereas the lower panel with blue shaded regions represents the allowed parameter space for IH and the cyan patch represents the area excluded by cosmology. Here from the $\sum m_i - \delta_{\text{CP}}$ (first column of Fig. 9) it is clear that *the bound on the absolute neutrino masses disallows some regions of the Dirac CP phase and $\sum m_i - \sin^2 \theta_{23}$, $\sin^2 \theta_{12}$ correlations are characteristics signature of this model.* From the third column of Fig. 9 we find that $\sin^2 \theta_{12}$ in FSS is restricted within a narrow range (the plot corresponds to the 3σ allowed range). The Majorana phases in our analysis, for the most general case, can be evaluated using the expressions given in Eq. (4.19) and (4.20) with the allowed regions of α , ϕ_{AC} , ϕ_{BC} given in Fig. 5 and 6. Thus we can constrain the Majorana phases using the low-energy neutrino oscillation data. In Fig. 10, present a correlation plot in the $\alpha_{21} - \alpha_{31}$ plane for NH (left panel, light red shaded region) and IH (right panel, blue shaded region) respectively with 3σ allowed ranges of neutrino oscillation data [5].

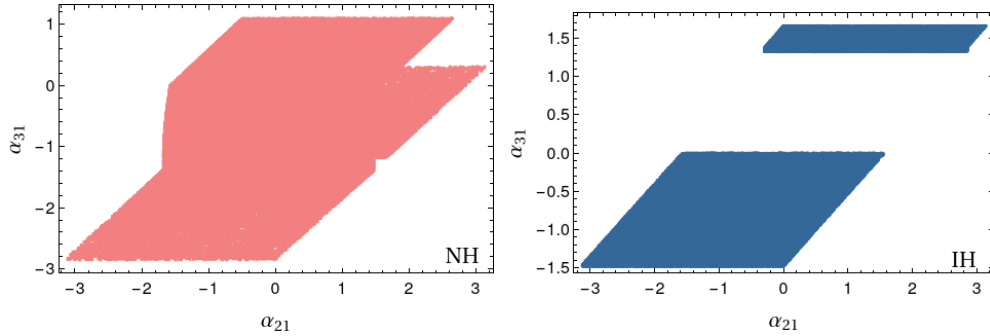


Figure 10. The correlation plot between two Majorana phases α_{21} and α_{31} for NH (left panel) and IH (right panel) for 3σ allowed range of neutrino oscillation data [5].

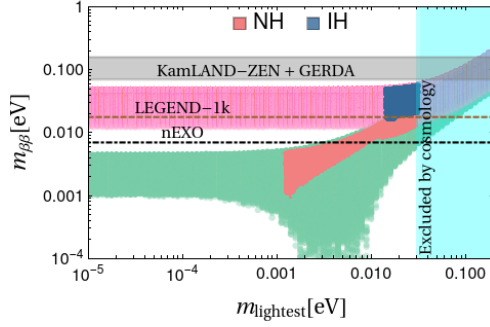


Figure 11. Neutrinoless double beta decay effective mass parameter $m_{\beta\beta}$ is plotted as a function of the lightest neutrino mass for the case of both NH (light red shaded region) and IH (blue shaded region). Green and magenta regions are three neutrino-allowed regions when all the parameters are varied within their 3σ range. The gray-shaded region, brown dashed, and black dotted-dash lines stand for experimental limits by KamLAND-Zen+GERDA, LEGEND-1k, and nEXO respectively. The vertical cyan area represents a disallowed region by cosmology.

Finally, with the estimation for neutrino masses and phases in hand, we are now able to plot the effective mass parameter characterizing neutrinoless double beta decay ($m_{\beta\beta}$) given in Eq. (5.2) and Eq. (5.3). In Fig. 11, we have plotted $m_{\beta\beta}$ against the lightest neutrino mass for both NH (m_1) and IH (m_3) respectively by light red and blue shaded regions respectively. The predictions for $m_{\beta\beta}$ are 1 – 30 meV for NH and 16-60 meV for IH. Here the green and magenta shaded regions represent 3σ allowed regions for the $m_{\beta\beta}$ predictions for NH and IH respectively. The vertical cyan-shaded regions represent the cosmological upper limit on the sum of absolute neutrino masses ($\sum m_i$). The gray shaded region represents the upper limit for $m_{\beta\beta}$ by combined analysis of KamLAND-Zen [146] and GERDA [147] experiments and predictions for $m_{\beta\beta}$ in our model fall within this upper limit. In this plot the brown dashed and black dotted-dash lines stand for future sensitivities of the LEGEND-1k [148] and nEXO [149] experiments respectively. Thus these near-future experiments have the potential to almost entirely falsify the IH prediction and probe a major part prediction for $m_{\beta\beta}$ for NH of light neutrino mass. Guided by the symmetry construction, the model also sets a lower limit on the effective mass parameter as $m_{\beta\beta} \geq 1$ meV for NH. Similar to Fig. 9, to obtain additional predictive correlations among neutrino masses and mixing, we plot a few more schematics. Thus in Fig. 12 we present the dependence of $m_{\beta\beta}$ on $\sin^2 \theta_{23}$, δ_{CP} , α_{21} and α_{31} for the FSS framework. Here the upper panel with light red shaded regions represents the allowed parameter space for NH. The lower panel with blue shaded regions represents the allowed parameter space for IH. Together with Fig. 9, the correlations between $\sum m_{\beta\beta}$ - δ_{CP} , \sin^2_{23} , α_{21} , α_{31} presented in Fig. 12 are typical features of FSS. The fate of the present model crucially depends on these correlations.

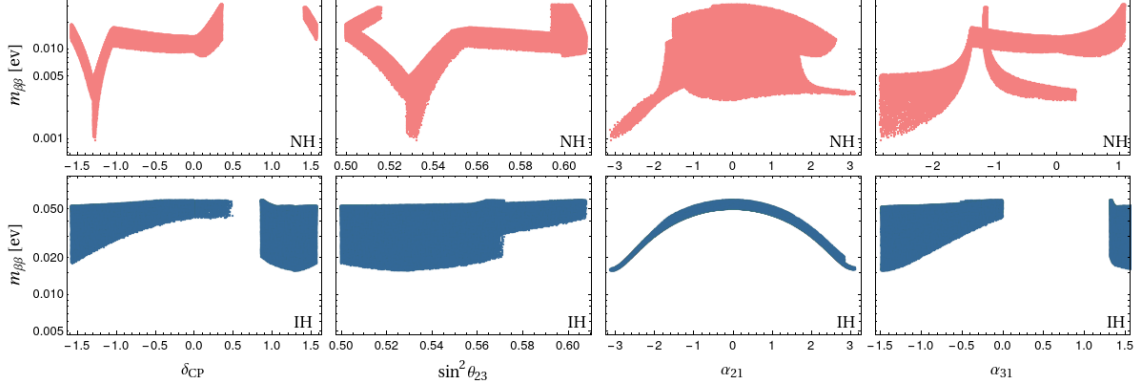


Figure 12. The correlation plot between $\sum m_i$ and δ_{CP} , \sin^2_{23} , α_{21} , α_{31} . The upper panels are schematics for NH whereas the lower panel is for IH.

Cases	NH	IH	δ_{CP}	α_{21}	α_{31}	$\sum m_i(\text{eV})$	$m_{\beta\beta}(\text{eV})$
Case I	\times	\checkmark	$0, \pi$	0	0	(0.1408, 0.1496)	(0.057, 0.059)
Case II	\times	\checkmark	$0, \pi$	$(0, 2\pi)$	0	(0.1408-0.1496)	(0.019-0.054)
Case III	\checkmark	\times	(0-0.78) (3.14, 3.66)	(-2.362, -1.26)	(0.61, 1.20)	(0.0773, 0.12)	(0.0059, 0.026)
Case IV	\checkmark	\times	(0, 0.78) (3.14, 3.66)	(0.60, 1.84)	(0.61, 1.20)	(0.0773, 0.12)	(0.013, 0.025)
General Case	\checkmark	\times	(-1.5, 0.6) (1.38, 1.57)	(-3, 3)	(-2.85, 1.13)	(0.06, 0.12)	(0.001, 0.03)
General Case	\times	\checkmark	(-1.5, 0.6) (0.8, 1.56)	(-3, 3)	(-1.5, -0.01) (1.33, 1.7)	(0.115, 0.15)	(0.016, 0.06)

Table 6. Summary of the different cases of our numerical analysis. The \checkmark and \times symbols stand for allowed and disallowed regimes. The numbers in the parenthesis represent the allowed ranges in each scenario.

To sum up the full numerical analysis, we present Table 6, where we give a summary of all the results including both special cases and general cases. In our analysis, we divided our special case into four categories depending on the values of the input relative phases ϕ_{AC} and ϕ_{BC} . In Case I, where $\phi_{AC} = \phi_{BC} = 0$, only IH of neutrino masses are allowed and $\delta_{CP} = 0$ or π , and two Majorana phases are coming out to be zero. In case II, where $\phi_{AC} = 0$ but $\phi_{BC} \neq 0$, IH is predicted and the main difference occurs in the prediction of Majorana phases. As a result, the prediction on $m_{\beta\beta}$ is different from Case I. In both Case III and Case IV where $\phi_{AC} = \phi_{BC} \neq 0$ and $\phi_{AC} \neq 0, \phi_{BC} = 0$, respectively, NH of neutrino masses are predicted. The allowed regions of δ_{CP} are given in Table 6 which are the same for both these cases. The prediction on the Majorana phase α_{31} is the same for both of these cases whereas the prediction on the α_{21} and hence $m_{\beta\beta}$ are different in both cases. Finally, as a most general case study, in Case V we vary ϕ_{AC} and

ϕ_{BC} arbitrarily within its full range. The analysis constrains δ_{CP} into two particular regions. We also find the values of the parameters β and the phase ϕ_{AC} plays a crucial role in determining the neutrino mass hierarchy with distinct limits on neutrino masses for each hierarchy.

6 Phenomenological implications for the FSS model

Owing to the flavor symmetry of the model, charged lepton sector's Yukawa couplings are diagonal so the flavors are conserved. But there are sources of the lepton flavor violation arising outside the charged lepton sector from both the Yukawa couplings y_N and y_s associated with the seesaw and scotogenic contributions, respectively. These Yukawa interactions lead to lepton flavor violating processes such as $l_\alpha \rightarrow l_\beta \gamma$, $l_\alpha \rightarrow 3l_\beta$ ($\alpha, \beta = e, \mu, \tau$) etc. For related studies on lepton flavor violation in a pure scotogenic model see [150–152]. Studies of such lepton flavor-violating processes in our framework depend heavily on the proposed symmetry configuration as described below.

In our framework, the branching ratios of the $l_\alpha \rightarrow l_\beta \gamma$ decays for the scotogenic contribution can be written as [102, 150]

$$\text{Br}(l_\alpha \rightarrow l_\beta \gamma) \approx \frac{3\pi\tilde{\alpha}}{64G_F^2} |Y_F^{\beta*} Y_F^\alpha|^2 \frac{1}{m_{\eta^+}^4} \left(F \left(\frac{M_f^2}{m_{\eta^+}^2} \right) \right)^2 \text{Br}(l_\alpha \rightarrow l_\beta \nu_\alpha \bar{\nu}_\beta). \quad (6.1)$$

Here G_F is the Fermi constant, $\tilde{\alpha} = e^2/4\pi$ is the fine structure constant. Y_F is the Yukawa coupling matrix coming from the scotogenic contribution given in Eq. (3.9). The expression for the function F is given by

$$F(x) = \frac{1 - 6x - 3x^2 + 2x^3 - 6x^2 \log x}{6(1-x)^4}. \quad (6.2)$$

In our discussion, considered discrete symmetries dictate the structure of the associated Yukawa couplings. Due to the specific VEV alignment of the A_4 triplet flavon ϕ_s and its contraction (following the multiplication rules given in the appendix) with the non-trivial A_4 singlet ξ (charged as $1'$), we find $Y_F^\mu = 0$ as given in Eq. (3.9). Therefore owing to the A_4 symmetry, the scotogenic part alone yields a vanishing contribution in the lepton flavor violating decays for $\mu \rightarrow e\gamma$ and $\tau \rightarrow \mu\gamma$. The only non-vanishing contribution arising in the $l_\alpha \rightarrow l_\beta \gamma$ decays originates from the $\tau \rightarrow e\gamma$ decay and the branching fraction can be written as

$$\text{Br}(\tau \rightarrow e\gamma) \approx \frac{3\pi\tilde{\alpha}}{64G_F^2} |-y_s y_s^* \epsilon^4|^2 \frac{1}{m_{\eta^+}^4} \left(F \left(\frac{M_f^2}{m_{\eta^+}^2} \right) \right)^2 \text{Br}(\tau \rightarrow e\nu_\tau \bar{\nu}_e), \quad (6.3)$$

$$= \frac{3\pi\alpha}{64G_F^2} \left(\frac{|C|}{\mathcal{F}(m_{\eta_R}, m_{\eta_I}, M_f)} \right)^2 \frac{1}{m_{\eta^+}^4} \left(F \left(\frac{M_f^2}{m_{\eta^+}^2} \right) \right)^2 \text{Br}(\tau \rightarrow e\nu_\tau \bar{\nu}_e) \quad (6.4)$$

In the above $\epsilon = v_f/\Lambda$ where we assume flavons VEVs to be equal, *i.e.*, $v_\xi = v_{s,a} = v_f$. There is also possible another type of the flavor violating decay $l_\alpha \rightarrow 3l_\beta$ ($l_\alpha \rightarrow l_\beta \bar{l}_\beta l_\beta$) and the corresponding

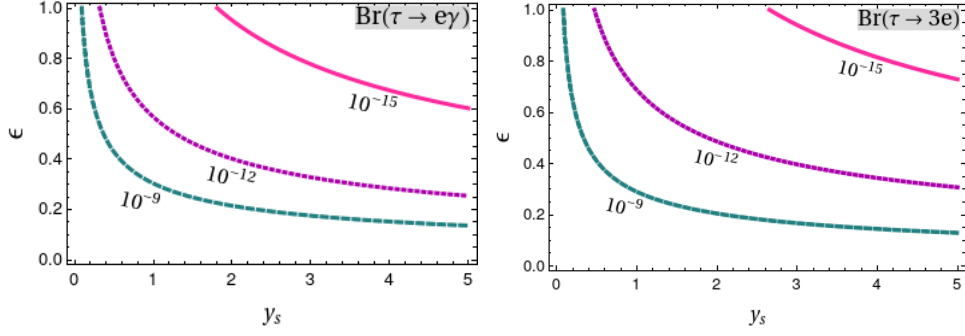


Figure 13. Contour plots for a branching fraction of $\tau \rightarrow e\gamma$ (left panel) and $\tau \rightarrow 3e$ (right panel) in the $y_s - \epsilon$ plane. The dashed, dotted, and continuous lines represent the branching fraction to be 10^{-9} , 10^{-12} , and 10^{-15} in both panels.

branching ratio is given by [150]

$$\text{Br}(l_\alpha \rightarrow 3l_\beta) \approx \frac{3\tilde{\alpha}^2}{512G_F^2} |Y_F^{\beta*} Y_F^\alpha|^2 \frac{1}{m_{\eta^+}^4} \mathcal{G}\left(\frac{m_\alpha}{m_\beta}\right) \left(F\left(\frac{M_f^2}{m_{\eta^+}^2}\right)\right)^2 \text{Br}(l_\alpha \rightarrow l_\beta \nu_\alpha \bar{\nu}_\beta). \quad (6.5)$$

where

$$\mathcal{G}\left(\frac{m_\alpha}{m_\beta}\right) = \left(\frac{16}{3} \log\left(\frac{m_\alpha}{m_\beta}\right) - \frac{22}{3}\right). \quad (6.6)$$

Since in FSS we have $Y_F^\mu = 0$, then branching fractions for $\mu \rightarrow 3e$ and $\tau \rightarrow 3\mu$ decays coming through the scotogenic contribution also vanishes. The only non-vanishing contribution originates from the $\tau \rightarrow 3e$ decay, and the branching fraction can be written as

$$\text{Br}(\tau \rightarrow 3e) \approx \frac{3\tilde{\alpha}^2}{512G_F^2} |-y_s y_s^* \epsilon^4|^2 \frac{1}{m_{\eta^+}^4} \mathcal{G}\left(\frac{m_\tau}{m_e}\right) \left(F\left(\frac{M_f^2}{m_{\eta^+}^2}\right)\right)^2 \text{Br}(\tau \rightarrow e \nu_\tau \bar{\nu}_e). \quad (6.7)$$

Clearly, from Eq. (6.3) and (6.7) we find with fixed values of the mass parameters that $\text{Br}(\tau \rightarrow e\gamma)$ and $\text{Br}(\tau \rightarrow 3e)$ depend upon y_s as well as ϵ (the ratio of flavon VEVs v_f to the cut-off scale Λ). Hence in Fig. 13 we present contour plots for the corresponding branching fractions in the $y_s - \epsilon$ plane considering $m_{\eta^+} = 600$ GeV and $M_f = 10$ TeV. The near future sensitivity of these two branching ratios is of the order of 10^{-9} [153]. Therefore we have plotted contours for the branching fraction of $\tau \rightarrow e\gamma$ (left panel) and $\tau \rightarrow 3e$ (right panel) fixed at 10^{-9} , 10^{-12} and 10^{-15} given by the dashed, dotted and continuous lines respectively. The $y_s - \epsilon$ correlation in Fig. 13 also helps us to estimate the ratio ϵ , and we find $\epsilon \leq 1$ since it is suppressed by the cut-off scale of the theory.

Now, for the type-I seesaw contribution in the lepton flavor violating decays, the decay of the form of $l_\alpha \rightarrow l_\beta \gamma$ will put a constraint on the FSS parameters. The branching ratio for such type

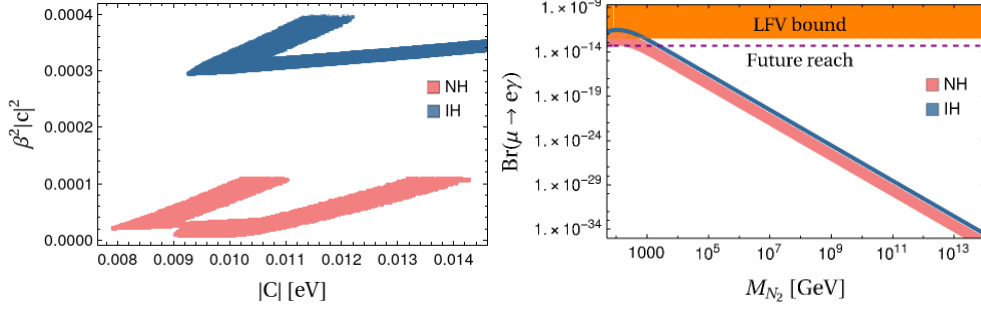


Figure 14. Left Panel : $\beta^2|C|^2$ vs $|C|$ for 3σ allowed regions of neutrino oscillation data obtained in Fig. 5 and Fig. 6. Right Panel: The branching ratio for $\mu \rightarrow e\gamma$ is plotted against the mass of the right-handed neutrino N_2 . The horizontal shaded region and the dashed line represent current and future experimental upper limits. In both panels light red, and blue shaded patches represent regions for NH and IH respectively.

of decay in our framework can be written as [154–158]

$$\text{Br}(l_\alpha \rightarrow l_\beta \gamma) \approx \frac{3\tilde{\alpha}v^4}{8\pi} \left| \sum_{i=1}^2 \mathcal{K}_{\beta i} \mathcal{K}_{i\alpha}^\dagger f\left(\frac{M_{N_i}^2}{M_W^2}\right) \right|^2, \quad (6.8)$$

$$= \sum_{i=1}^2 \frac{3\tilde{\alpha}v^4}{8\pi M_{N_i}^4} \left| (Y_N)_{\beta i} (Y_N^\dagger)_{i\alpha} f\left(\frac{M_{N_i}^2}{M_W^2}\right) \right|^2 \quad (6.9)$$

where $\mathcal{K} = Y_N^\dagger (M_R^{-1})^*$ and $Y_N = M_D/v$, as obtained from Eq. (3.4). Similarly to the scotogenic contribution, the VEV alignment of the A_4 flavon ϕ_s once again plays a crucial role in obtaining the estimation for the branching ratio $l_\alpha \rightarrow l_\beta \gamma$ decays. The VEV configuration of ϕ_s is such that it gives rise to $(Y_N)_{e1} = 0$ (see Eq. (3.4)) and the contribution associated with N_1 essentially vanishes for $\mu \rightarrow e\gamma$ and $\tau \rightarrow e\gamma$. Therefore only surviving contribution in these decays originates from N_2 . Again due to the A_4 flavor symmetry we find $(Y_N)_{e2} = (Y_N)_{\mu 2} = (Y_N)_{\tau 2}$ as written in the second column of M_D , see Eq. (3.4). As a result, the expression for the branching fraction for the above two decays will be the same *i.e.*, $\text{Br}(\mu \rightarrow e\gamma) = \text{Br}(\tau \rightarrow e\gamma)$. Out of these two decays, the most stringent constraint comes from the $\mu \rightarrow e\gamma$ decay and in the following, we discuss the numerical analysis for the same. Following Eq. (6.9), in our framework, the branching ratio of $\mu \rightarrow e\gamma$ can be written as

$$\text{Br}(\mu \rightarrow e\gamma) = \frac{3\tilde{\alpha}v^4}{8\pi M_{N_2}^4} \left| (y_{N_2} y_{N_2}^* \epsilon^2 f\left(\frac{M_{N_2}^2}{M_W^2}\right)) \right|^2 = \frac{3\tilde{\alpha}}{8\pi M_{N_2}^2} \beta^2 |C|^2 \left(f\left(\frac{M_{N_2}^2}{M_W^2}\right) \right)^2. \quad (6.10)$$

where we have used $B = v^2 y_{N_2}^2 \epsilon^2 / M_{N_2}$ from Eq. (3.6) and the definition $\beta = |B|/|C|$ to obtain Eq. (6.10). The loop function $f(x)$ in Eq. (6.10) can be written as

$$f(x) = \frac{x(2x^3 + 3x^2 - 6x - 6x^2 \log(x) + 1)}{2(1-x)^4}. \quad (6.11)$$

From Eq. (6.10) we find that the contribution in $\text{Br}(\mu \rightarrow e\gamma)$ coming from the seesaw mechanism depends on the mass of the heavy right-handed neutrino N_2 , β and $|C|$. The parameters β and

$|C|$ are already fixed by neutrino data, as discussed in Section 5. As $\text{Br}(\mu \rightarrow e\gamma) \propto \beta^2|C|^2$, in Fig. 14 left panel we have shown the variation of $\beta^2|C|^2$ with $|C|$ for the most general case of our analysis. In this plot, the light red and blue shaded regions represent an estimation for $\beta^2|C|^2$ as a function of $|C|$ for NH and IH light neutrino masses, respectively. Furthermore, Fig. 14 left panel also depicts that $\beta^2|C|^2$ acquires higher values for IH compared to NH. This is because for NH β is smaller ($\beta \leq 1$) compared to IH ($\beta \geq 1$) for similar values of $|C|$. With this when we plot $\text{Br}(\mu \rightarrow e\gamma)$ for seesaw contribution in our scenario as a function of M_{N_2} in the right panel of Fig. 14. Here the light red and blue shaded region represent prediction for $\text{Br}(\mu \rightarrow e\gamma)$ for NH and IH of light neutrino mass. As the $\beta^2|C|^2$ takes higher values for IH compared to NH, the branching ratio for the $\mu \rightarrow e\gamma$ decay is higher for IH compared to NH as seen in this figure. The horizontal orange shaded region represents current experimental limit $\text{Br}(\mu \rightarrow e\gamma) \leq 4.2 \times 10^{-13}$ [159] and the purple dashed stands for the future reach $\text{Br}(\mu \rightarrow e\gamma) \leq 6 \times 10^{-14}$ [160] which puts a lower limit on the mass of N_2 in the range $0.2 \text{ TeV} \leq M_{N_2} \leq 1.6 \text{ TeV}$ ($1.7 \text{ TeV} \leq M_{N_2} \leq 3 \text{ TeV}$) for NH (IH) of light neutrino mass. Again, following Eq. (6.9), the branching ratio for $\tau \rightarrow \mu\gamma$ in case of the seesaw contribution can be expressed as

$$\text{Br}(\tau \rightarrow \mu\gamma) = \sum_{i=1}^2 \frac{3\tilde{\alpha}v^4}{8\pi M_{N_i}^4} \left| (Y_N)_{\tau i} (Y_N^\dagger)_{i\mu} f\left(\frac{M_{N_i}^2}{M_W^2}\right) \right|^2, \quad (6.12)$$

$$= \frac{3\tilde{\alpha}}{8\pi M_{N_1}^2} \alpha^2 |C|^2 \left(f\left(\frac{M_{N_1}^2}{M_W^2}\right) \right)^2 + \frac{3\tilde{\alpha}}{8\pi M_{N_2}^2} \beta^2 |C|^2 \left(f\left(\frac{M_{N_2}^2}{M_W^2}\right) \right)^2. \quad (6.13)$$

where we have used the relations $A = v^2 y_{N_1}^2 \epsilon^2 / M_{N_1}$ and $\alpha = |A|/|C|$. Thus the contribution to

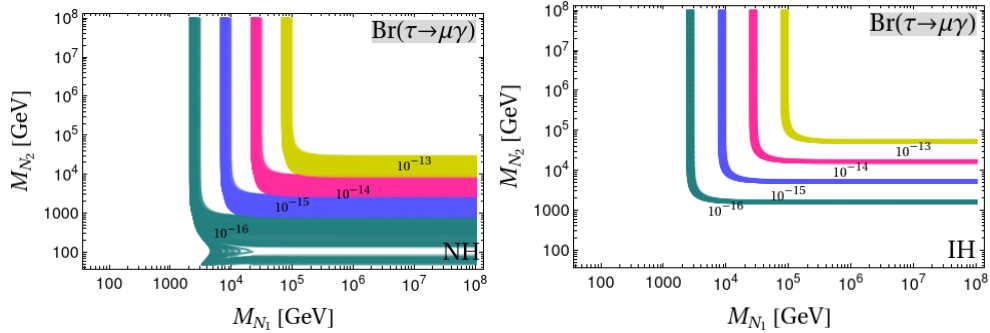


Figure 15. Contour plot for branching fraction of $\mu \rightarrow e\gamma$ (fixed at 10^{-13} , 10^{-14} , 10^{-15} , 10^{-16} respectively) in the M_{N_1} - M_{N_2} plane. The left and right panels represent allowed regions (obtained from Fig. 5) for NH and IH respectively.

$\text{Br}(\tau \rightarrow \mu\gamma)$ coming from the seesaw mechanism depends on the masses of the heavy right-handed neutrinos $N_{1,2}$ as well as α, β and $|C|$. The parameters α, β , and $|C|$ are already fixed to satisfy correct neutrino oscillation data as discussed in Section 5. Hence in Fig. 15 we have plotted different contours for $\text{Br}(\tau \rightarrow \mu\gamma)$ in the M_{N_1} - M_{N_2} plane, corresponding to the 3σ allowed range of

neutrino data for both NH and IH. In two panels, we have plotted the contours showing the M_{N_1} - M_{N_2} correlations with branching fractions fixed at 10^{-13} , 10^{-14} , 10^{-15} and 10^{-16} (given by yellow, magenta, blue and green regions respectively). Here it is worth mentioning that among $l_\alpha \rightarrow l_\beta \gamma$ decays, as a consequence of the flavor symmetric construction, only the seesaw part contributes to the $\mu \rightarrow e \gamma$ and $\tau \rightarrow \mu \gamma$ decays. Whereas in the branching fraction of the decay $\tau \rightarrow e \gamma$, both scotogenic and seesaw parts contribute. To understand the relative magnitude of these two contributions involved in the $\tau \rightarrow e \gamma$ decay, we define a ratio R as

$$R = \frac{\text{Br}(\tau \rightarrow e \gamma)_{\text{scoto}}}{\text{Br}(\tau \rightarrow e \gamma)_{\text{seesaw}}}. \quad (6.14)$$

Now following Eq. (6.3) and Eq. (6.10) along with Eq. (3.10), in the FSS framework we find that the ratio R is proportional to $1/\beta^2$ for specific values of the scoto-seesaw mass parameters. In Fig. 16,

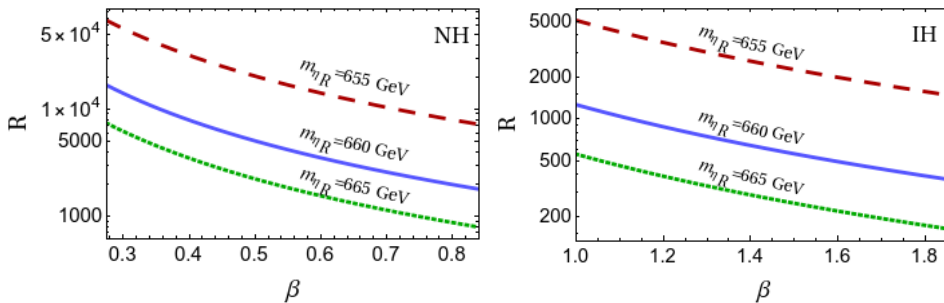


Figure 16. The ratio (R) of the branching fractions for the scoto and seesaw contributions versus β for both NH (left panel) and IH (right panel).

we have plotted R considering $m_{\eta^+} = 600$ GeV, $m_{\eta_I} = 650$ GeV, $M_f = 10^5$ GeV, and $M_{N_2} = 10^6$ GeV for both NH (left panel) and IH (right panel) respectively. In the panels, the brown dashed, blue continuous, and green dotted lines represent the estimation for R with $m_{\eta_R} = 655$ GeV, 660 GeV, and 665 GeV respectively. These lines correspond to the allowed range for β obtained earlier. Since $R \geq 10^3$ ($R \geq 2 \times 10^2$) for NH (IH), we can conclude that the scotogenic part dominates the seesaw contribution in the lepton flavor violating decay such as $\tau \rightarrow e \gamma$.

The scotogenic contribution in our analysis offers us the opportunity to explain the nature of dark matter. In this model, there is an inherent dark \mathcal{Z}_2 symmetry that ensures the stability of the lightest dark particle, and three feasible dark matter candidates exist. These are, namely, the fermionic dark matter f and scalar dark matter, which are real and imaginary components of η , given by η_R and η_I , respectively. When the lightest dark particle originates from η , it resembles the inert Higgs doublet model [161]. Considering η_R as the DM candidate, there exists several annihilation and co-annihilation channels in this model which involve annihilation to quarks and leptons, SM gauge bosons, and the Higgs boson such as $\eta_R \eta_R \rightarrow ZZ$, $W^+ W^-$, hh , $q\bar{q}$ etc. Collectively they all contribute to the relic abundance of η_R . Present dark matter abundance is often expressed in

terms of the relic density parameter $\Omega^2 h$ and reported to be $\Omega^2 h = 0.120 \pm 0.001$ at 68% CL [162]. In a minimal scoto-seesaw framework [108], it has been argued that correct relic density can be obtained for three different mass ranges for η_R . These are respectively $m_{\eta_R} < 50$ GeV, $70 \text{ GeV} < m_{\eta_R} < 100$ GeV and $m_{\eta_R} > 550$ GeV. The dark matter mass in the range $m_{\eta_R} < 50$ is disallowed as it is in conflict with the LHC Higgs invisible decay limit [163]. The intermediate region $70 \text{ GeV} < m_{\eta_R} < 100$ GeV is not completely ruled out by the LHC and LEP data and dark matter mass in the range $m_{\eta_R} > 550$ GeV is not affected by the collider constraints. The phenomenology of fermionic dark matter is worth exploring and is beyond the scope of the current study.

7 Conclusions

We have proposed the flavor-scoto-seesaw (FSS) model that establishes a common origin of the nonzero θ_{13} and cosmological dark matter. The framework is based on the A_4 flavor symmetry where both type-I seesaw and scotogenic mechanisms contribute to the effective light neutrino mass. FSS explains observed neutrino masses and mixing angles provides rich phenomenology and accommodates potential dark matter candidates. Guided by the discrete symmetry, we show that the minimal type-I seesaw first reproduces the widely popular TBM mixing, a first-order approximation of the lepton mixing matrix. Subsequently, the scotogenic contribution acts as a requisite deviation to the TBM mixing and addresses the issue of the nature of dark matter. We also demonstrate that the neutrino mixing pattern exhibits TM_2 mixing scheme (a viable descendent of the TBM mixing pattern) within this scoto-seesaw scenario.

The model which we construct here is highly predictive in nature. Using the current experimental observation on neutrino oscillation and other cosmological limits, *we found that the allowed parameter space in the FSS model restricts some of the key observables associated with neutrinos (the atmospheric mixing angle, Dirac and Majorana CP phases, effective mass parameter appearing in the neutrinoless double beta decay) and crucially dictates the lepton flavor violating decays.* To understand the behaviours of the parameters involved (namely, $\alpha, \beta, \phi_{AC}, \phi_{BC}$), we divide the numerical analysis into a few specific cases based on the choice of the associated phases (ϕ_{AC}, ϕ_{BC}) and then carried out the complete general numerical analysis. These limiting cases can easily distinguish between light neutrino masses' normal and inverted hierarchy. For example, when the relative phase between the seesaw contribution associated with right-handed neutrino N_1 and the scotogenic contribution is considered zero (*i.e.*, $\phi_{AC} = 0$ for Case I and II), only inverted hierarchy is allowed. On the other hand, when $\phi_{AC} \neq 0$ (Case III and IV), only normal hierarchy is allowed. Considered discrete flavor symmetries play an instrumental role in producing such distinctive constraints. Subsequently, for the most general case, we carried out the numerical analysis for all possible choices of the parameters involved and found that normal hierarchy can be realized

only with $\beta \leq 1$ and $2.61 \leq \phi_{AC} \leq 5.38$ whereas to realize inverted hierarchy we need $\beta \geq 1$ and $0 \leq \phi_{AC} \leq 2$ (or $6 \leq \phi_{AC} \leq 2\pi$). This analysis also predicts the atmospheric mixing angle lying in the upper octant, in good agreement with the latest global fit neutrino oscillation data, and restricts Dirac CP phase δ_{CP} within $-1.57 \leq \delta_{CP} \leq 1.37$ (and $1.4 \leq \delta_{CP} \leq 1.57$) for normal hierarchy and $-1.57 \leq \delta_{CP} \leq 0.5$ (and $0.86 \leq \delta_{CP} \leq 1.57$) for inverted hierarchy. Along with the Dirac CP phase δ_{CP} , the Majorana phases also get restricted in our analysis. Furthermore, we obtain a lower limit on the lightest neutrino mass as $m_{\text{lightest}} \geq 0.0012$ eV for normal hierarchy and $m_{\text{lightest}} \geq 0.014$ eV for inverted hierarchy. We have also estimated the prediction for the effective mass parameter $m_{\beta\beta}$ characterizing the neutrinoless double beta decay and found it to be in the range $1 - 30$ meV for normal hierarchy and $16 - 60$ meV for inverted hierarchy, respectively. These values are within the reach of future neutrinoless double beta decay experiments. The unique prediction on the correlation among the masses and mixing such as $m_{\beta\beta}$ - δ_{CP} , $\sin_{23}^2, \alpha_{21}, \alpha_{31}$ as well as $\sum m_i$ - δ_{CP} , \sin_{23}^2 , etc. are typical features of the discussed FSS model. For example, the sum of absolute neutrino masses crucially dictates the allowed ranges for δ_{CP} mentioned above. In the end, we also comment on the phenomenological implications, such as lepton flavor violation and the prospects of dark matter candidates in such a scenario. As a consequence of the flavor structure, the scotogenic part of the model does not contribute to the lepton flavor violating decays such as $\mu \rightarrow e\gamma$ and $\tau \rightarrow \mu\gamma$, and a lower limit on the mass of the heavy right-handed neutrinos can be obtained from the constraints on the branching ratios involving such decays. On the other hand, both scoto and seesaw parts contribute to the decay $\tau \rightarrow e\gamma$. However, the scotogenic part dominates this rare decay and a constraint on the ratio of flavon VEVs to the cut-off scale of the theory can be obtained. A detailed discussion of the phenomenological aspects in this direction is dedicated to future investigations.

Appendix: A_4 symmetry

A_4 is a discrete group of even permutations of four objects³. Geometrically, it is an invariance group of a tetrahedron. It has 12 elements which can be generated by two basic objects S and T which obey the following relation

$$S^2 = T^3 = (ST)^3 = 1 \quad (7.1)$$

The A_4 group has three one-dimensional irreducible representations $1, 1'$ and $1''$ and one three dimensional irreducible representation 3 . Products of the singlets and triplets are given by

$$1 \otimes 1 = 1; \quad 1' \otimes 1'' = 1, \quad (7.2)$$

$$1' \otimes 1' = 1''; \quad 1'' \otimes 1'' = 1', \quad (7.3)$$

$$3 \otimes 3 = 1 \oplus 1' \oplus 1'' \oplus 3_s \oplus 3_a, \quad (7.4)$$

³For a detailed discussion on A_4 see Ref. [19, 20]

where the subscripts “s” and “a” denote symmetric and antisymmetric part respectively. Writing two triplets as (x_1, x_2, x_3) and (y_1, y_2, y_3) respectively, their products are given by

$$1 \sim x_1 y_1 + x_2 y_3 + x_3 y_2, \quad (7.5)$$

$$1' \sim x_3 y_3 + x_1 y_2 + x_2 y_1, \quad (7.6)$$

$$1'' \sim x_2 y_2 + x_1 y_3 + x_3 y_1, \quad (7.7)$$

$$3_s \sim \begin{pmatrix} 2x_1 y_1 - x_2 y_3 - x_3 y_2 \\ 2x_3 y_3 - x_1 y_2 - x_2 y_1 \\ 2x_2 y_2 - x_1 y_3 - x_3 y_1 \end{pmatrix}, \quad (7.8)$$

$$3_a \sim \begin{pmatrix} x_2 y_3 - x_3 y_2 \\ x_1 y_2 - x_2 y_1 \\ x_3 y_1 - x_1 y_3 \end{pmatrix}. \quad (7.9)$$

Acknowledgments

This work has been supported in part by the Polish National Science Center (NCN) under grant 2020/37/B/ST2/02371 and the Freedom of Research (Swoboda Badań) initiative of the University of Silesia in Katowice. BK would like to thank José W. F. Valle for useful discussions.

References

- [1] B. Pontecorvo, *Neutrino Experiments and the Problem of Conservation of Leptonic Charge*, *Zh. Eksp. Teor. Fiz.* **53** (1967) 1717.
- [2] SNO collaboration, *Measurement of the rate of $\nu_e + d \rightarrow p + p + e^-$ interactions produced by ^8B solar neutrinos at the Sudbury Neutrino Observatory*, *Phys. Rev. Lett.* **87** (2001) 071301 [[nucl-ex/0106015](#)].
- [3] SUPER-KAMIOKANDE collaboration, *Evidence for oscillation of atmospheric neutrinos*, *Phys. Rev. Lett.* **81** (1998) 1562 [[hep-ex/9807003](#)].
- [4] M.C. Gonzalez-Garcia and M. Maltoni, *Phenomenology with Massive Neutrinos*, *Phys. Rept.* **460** (2008) 1 [[0704.1800](#)].
- [5] P.F. de Salas, D.V. Forero, S. Gariazzo, P. Martínez-Miravé, O. Mena, C.A. Ternes et al., *2020 global reassessment of the neutrino oscillation picture*, *JHEP* **02** (2021) 071 [[2006.11237](#)].
- [6] WMAP collaboration, *Nine-Year Wilkinson Microwave Anisotropy Probe (WMAP) Observations: Cosmological Parameter Results*, *Astrophys. J. Suppl.* **208** (2013) 19 [[1212.5226](#)].
- [7] PLANCK collaboration, *Planck 2018 results. VI. Cosmological parameters*, *Astron. Astrophys.* **641** (2020) A6 [[1807.06209](#)].

- [8] G. Bertone, D. Hooper and J. Silk, *Particle dark matter: Evidence, candidates and constraints*, *Phys. Rept.* **405** (2005) 279 [[hep-ph/0404175](#)].
- [9] P. Minkowski, $\mu \rightarrow e\gamma$ at a Rate of One Out of 10^9 Muon Decays?, *Phys. Lett. B* **67** (1977) 421.
- [10] M. Gell-Mann, P. Ramond and R. Slansky, *Complex Spinors and Unified Theories*, *Conf. Proc. C* **790927** (1979) 315 [[1306.4669](#)].
- [11] R.N. Mohapatra and G. Senjanovic, *Neutrino Mass and Spontaneous Parity Violation*, *Phys. Rev. Lett.* **44** (1980) 912.
- [12] J. Schechter and J.W.F. Valle, *Neutrino Decay and Spontaneous Violation of Lepton Number*, *Phys. Rev. D* **25** (1982) 774.
- [13] J. Schechter and J.W.F. Valle, *Neutrino Masses in $SU(2) \times U(1)$ Theories*, *Phys. Rev.* **D22** (1980) 2227.
- [14] S.F. King, *Neutrino Mass and Mixing in the Seesaw Playground*, *Nucl. Phys. B* **908** (2016) 456 [[1511.03831](#)].
- [15] Z.-z. Xing and Z.-h. Zhao, *The minimal seesaw and leptogenesis models*, *Rept. Prog. Phys.* **84** (2021) 066201 [[2008.12090](#)].
- [16] S.F. King, *Large mixing angle MSW and atmospheric neutrinos from single right-handed neutrino dominance and $U(1)$ family symmetry*, *Nucl. Phys. B* **576** (2000) 85 [[hep-ph/9912492](#)].
- [17] S.F. King, *Constructing the large mixing angle MNS matrix in seesaw models with right-handed neutrino dominance*, *JHEP* **09** (2002) 011 [[hep-ph/0204360](#)].
- [18] S. Morisi and J.W.F. Valle, *Neutrino masses and mixing: a flavour symmetry roadmap*, *Fortsch. Phys.* **61** (2013) 466 [[1206.6678](#)].
- [19] H. Ishimori, T. Kobayashi, H. Ohki, Y. Shimizu, H. Okada and M. Tanimoto, *Non-Abelian Discrete Symmetries in Particle Physics*, *Prog. Theor. Phys. Suppl.* **183** (2010) 1 [[1003.3552](#)].
- [20] G. Altarelli and F. Feruglio, *Discrete Flavor Symmetries and Models of Neutrino Mixing*, *Rev. Mod. Phys.* **82** (2010) 2701 [[1002.0211](#)].
- [21] F. Feruglio and A. Romanino, *Lepton flavor symmetries*, *Rev. Mod. Phys.* **93** (2021) 015007 [[1912.06028](#)].
- [22] S.F. King and C. Luhn, *Neutrino Mass and Mixing with Discrete Symmetry*, *Rept. Prog. Phys.* **76** (2013) 056201 [[1301.1340](#)].
- [23] S.T. Petcov, *Discrete Flavour Symmetries, Neutrino Mixing and Leptonic CP Violation*, *Eur. Phys. J. C* **78** (2018) 709 [[1711.10806](#)].
- [24] Z.-z. Xing, *Flavor structures of charged fermions and massive neutrinos*, *Phys. Rept.* **854** (2020) 1 [[1909.09610](#)].

- [25] G. Chauhan, P.S.B. Dev, B. Dzierwit, W. Flieger, J. Gluza, K. Grzanka et al., *Discrete Flavor Symmetries and Lepton Masses and Mixings*, in *2022 Snowmass Summer Study*, 3, 2022 [[2203.08105](#)].
- [26] F. Vissani, *A Study of the scenario with nearly degenerate Majorana neutrinos*, [hep-ph/9708483](#).
- [27] V.D. Barger, S. Pakvasa, T.J. Weiler and K. Whisnant, *Bimaximal mixing of three neutrinos*, *Phys. Lett. B* **437** (1998) 107 [[hep-ph/9806387](#)].
- [28] A. Datta, F.-S. Ling and P. Ramond, *Correlated hierarchy, Dirac masses and large mixing angles*, *Nucl. Phys. B* **671** (2003) 383 [[hep-ph/0306002](#)].
- [29] Y. Kajiyama, M. Raidal and A. Strumia, *The Golden ratio prediction for the solar neutrino mixing*, *Phys. Rev. D* **76** (2007) 117301 [[0705.4559](#)].
- [30] C.H. Albright, A. Dueck and W. Rodejohann, *Possible Alternatives to Tri-bimaximal Mixing*, *Eur. Phys. J. C* **70** (2010) 1099 [[1004.2798](#)].
- [31] P.F. Harrison, D.H. Perkins and W.G. Scott, *Tri-bimaximal mixing and the neutrino oscillation data*, *Phys. Lett.* **B530** (2002) 167 [[hep-ph/0202074](#)].
- [32] P.F. Harrison and W.G. Scott, *Symmetries and generalizations of tri - bimaximal neutrino mixing*, *Phys. Lett.* **B535** (2002) 163 [[hep-ph/0203209](#)].
- [33] S. Chang, S.K. Kang and K. Siyeon, *Minimal seesaw model with tri/bi-maximal mixing and leptogenesis*, *Phys. Lett. B* **597** (2004) 78 [[hep-ph/0404187](#)].
- [34] N.W. Park, K.H. Nam and K. Siyeon, *Discrete flavor symmetry and minimal seesaw mechanism*, *Phys. Rev. D* **83** (2011) 056013 [[1101.4134](#)].
- [35] Z.-h. Zhao, *Realizing Tri-bimaximal Mixing in Minimal Seesaw Model with S_4 Family Symmetry*, *Phys. Lett. B* **701** (2011) 609 [[1106.2715](#)].
- [36] S.F. King, *Atmospheric and solar neutrinos from single right-handed neutrino dominance and $U(1)$ family symmetry*, *Nucl. Phys. B* **562** (1999) 57 [[hep-ph/9904210](#)].
- [37] E. Ma and G. Rajasekaran, *Softly broken $A(4)$ symmetry for nearly degenerate neutrino masses*, *Phys. Rev.* **D64** (2001) 113012 [[hep-ph/0106291](#)].
- [38] E. Ma, *$A(4)$ symmetry and neutrinos with very different masses*, *Phys. Rev. D* **70** (2004) 031901 [[hep-ph/0404199](#)].
- [39] E. Ma, *Quark mass matrices in the $A(4)$ model*, *Mod. Phys. Lett.* **A17** (2002) 627 [[hep-ph/0203238](#)].
- [40] G. Altarelli and F. Feruglio, *Tri-bimaximal neutrino mixing from discrete symmetry in extra dimensions*, *Nucl. Phys. B* **720** (2005) 64 [[hep-ph/0504165](#)].
- [41] G. Altarelli and F. Feruglio, *Tri-bimaximal neutrino mixing, $A(4)$ and the modular symmetry*, *Nucl. Phys. B* **741** (2006) 215 [[hep-ph/0512103](#)].

- [42] K.S. Babu, E. Ma and J.W.F. Valle, *Underlying $A(4)$ symmetry for the neutrino mass matrix and the quark mixing matrix*, *Phys. Lett. B* **552** (2003) 207 [[hep-ph/0206292](#)].
- [43] DOUBLE CHOOZ collaboration, *Indication for the disappearance of reactor electron antineutrinos in the Double Chooz experiment*, *Phys. Rev. Lett.* **108** (2012) 131801 [[1112.6353](#)].
- [44] DAYA BAY collaboration, *Observation of electron-antineutrino disappearance at Daya Bay*, *Phys. Rev. Lett.* **108** (2012) 171803 [[1203.1669](#)].
- [45] RENO collaboration, *Observation of Reactor Electron Antineutrino Disappearance in the RENO Experiment*, *Phys. Rev. Lett.* **108** (2012) 191802 [[1204.0626](#)].
- [46] T2K collaboration, *Observation of Electron Neutrino Appearance in a Muon Neutrino Beam*, *Phys. Rev. Lett.* **112** (2014) 061802 [[1311.4750](#)].
- [47] MINOS collaboration, *Measurement of Neutrino and Antineutrino Oscillations Using Beam and Atmospheric Data in MINOS*, *Phys. Rev. Lett.* **110** (2013) 251801 [[1304.6335](#)].
- [48] B. Adhikary and A. Ghosal, *Nonzero $U(e3)$, CP violation and leptogenesis in a see-saw type softly broken $A(4)$ symmetric model*, *Phys. Rev. D* **78** (2008) 073007 [[0803.3582](#)].
- [49] B. Brahmachari, S. Choubey and M. Mitra, *The $A(4)$ flavor symmetry and neutrino phenomenology*, *Phys. Rev. D* **77** (2008) 073008 [[0801.3554](#)].
- [50] S.F. King, *Tri-bimaximal Neutrino Mixing and θ_{13}* , *Phys. Lett. B* **675** (2009) 347 [[0903.3199](#)].
- [51] G. Branco, R. Gonzalez Felipe, M. Rebelo and H. Serodio, *Resonant leptogenesis and tribimaximal leptonic mixing with $A(4)$ symmetry*, *Phys. Rev. D* **79** (2009) 093008 [[0904.3076](#)].
- [52] D. Aristizabal Sierra, F. Bazzocchi, I. de Medeiros Varzielas, L. Merlo and S. Morisi, *Tri-Bimaximal Lepton Mixing and Leptogenesis*, *Nucl. Phys. B* **827** (2010) 34 [[0908.0907](#)].
- [53] S. Morisi and E. Peinado, *An $A(4)$ model for lepton masses and mixings*, *Phys. Rev. D* **80** (2009) 113011 [[0910.4389](#)].
- [54] Y.H. Ahn, H.-Y. Cheng and S. Oh, *Quark-lepton complementarity and tribimaximal neutrino mixing from discrete symmetry*, *Phys. Rev. D* **83** (2011) 076012 [[1102.0879](#)].
- [55] Y. Shimizu, M. Tanimoto and A. Watanabe, *Breaking Tri-bimaximal Mixing and Large θ_{13}* , *Prog. Theor. Phys.* **126** (2011) 81 [[1105.2929](#)].
- [56] J. Ganguly and R.S. Hundi, *Neutrino Mixing by modifying the Yukawa coupling structure of constrained sequential dominance*, *Phys. Rev. D* **103** (2021) 035007 [[2005.04023](#)].
- [57] J. Ganguly and R.S. Hundi, *Deviation from tri-bimaximal mixing as a result of modification of Yukawa coupling structure of constrained sequential dominance*, *J. Phys. Conf. Ser.* **2156** (2021) 012183.
- [58] Y.H. Ahn, H.-Y. Cheng and S. Oh, *An extension of tribimaximal lepton mixing*, *Phys. Rev. D* **84** (2011) 113007 [[1107.4549](#)].

- [59] S. Antusch, S.F. King, C. Luhn and M. Spinrath, *Trimaximal mixing with predicted θ_{13} from a new type of constrained sequential dominance*, *Nucl. Phys. B* **856** (2012) 328 [[1108.4278](#)].
- [60] D. Borah, B. Karmakar and D. Nanda, *Planck scale origin of nonzero θ_{13} and super-WIMP dark matter*, *Phys. Rev. D* **100** (2019) 055014 [[1906.02756](#)].
- [61] G.-J. Ding and D. Meloni, *A Model for Tri-bimaximal Mixing from a Completely Broken A_4* , *Nucl. Phys. B* **855** (2012) 21 [[1108.2733](#)].
- [62] S.F. King and C. Luhn, *A_4 models of tri-bimaximal-reactor mixing*, *JHEP* **03** (2012) 036 [[1112.1959](#)].
- [63] A. Mukherjee and M.K. Das, *Neutrino phenomenology and scalar Dark Matter with A_4 flavor symmetry in Inverse and type II seesaw*, *Nucl. Phys. B* **913** (2016) 643 [[1512.02384](#)].
- [64] I. de Medeiros Varzielas and L. Merlo, *Ultraviolet Completion of Flavour Models*, *JHEP* **02** (2011) 062 [[1011.6662](#)].
- [65] Y.H. Ahn and H. Okada, *Non-zero θ_{13} linking to Dark Matter from Non-Abelian Discrete Flavor Model in Radiative Seesaw*, *Phys. Rev. D* **85** (2012) 073010 [[1201.4436](#)].
- [66] Y.H. Ahn and S.K. Kang, *Non-zero θ_{13} and CP violation in a model with A_4 flavor symmetry*, *Phys. Rev. D* **86** (2012) 093003 [[1203.4185](#)].
- [67] Y. BenTov, X.-G. He and A. Zee, *An $A_4 \times Z_4$ model for neutrino mixing*, *JHEP* **12** (2012) 093 [[1208.1062](#)].
- [68] G.C. Branco, R. Gonzalez Felipe, F.R. Joaquim and H. Serodio, *Spontaneous leptonic CP violation and nonzero θ_{13}* , *Phys. Rev. D* **86** (2012) 076008 [[1203.2646](#)].
- [69] D. Borah, M.K. Das and A. Mukherjee, *Common origin of nonzero θ_{13} and baryon asymmetry of the Universe in a TeV scale seesaw model with A_4 flavor symmetry*, *Phys. Rev. D* **97** (2018) 115009 [[1711.02445](#)].
- [70] A.E. Carcamo Hernandez, I. de Medeiros Varzielas, S.G. Kovalenko, H. Päs and I. Schmidt, *Lepton masses and mixings in an A_4 multi-Higgs model with a radiative seesaw mechanism*, *Phys. Rev. D* **88** (2013) 076014 [[1307.6499](#)].
- [71] S. Bhattacharya, B. Karmakar, N. Sahu and A. Sil, *Flavor origin of dark matter and its relation with leptonic nonzero θ_{13} and Dirac CP phase δ* , *JHEP* **05** (2017) 068 [[1611.07419](#)].
- [72] J. Barry and W. Rodejohann, *Deviations from tribimaximal mixing due to the vacuum expectation value misalignment in A_4 models*, *Phys. Rev. D* **81** (2010) 093002 [[1003.2385](#)].
- [73] M.-C. Chen, J. Huang, J.-M. O'Bryan, A.M. Wijangco and F. Yu, *Compatibility of θ_{13} and the Type I Seesaw Model with A_4 Symmetry*, *JHEP* **02** (2013) 021 [[1210.6982](#)].
- [74] B. Karmakar and A. Sil, *An A_4 realization of inverse seesaw: neutrino masses, θ_{13} and leptonic non-unitarity*, *Phys. Rev. D* **96** (2017) 015007 [[1610.01909](#)].

- [75] Z.-h. Zhao, *Minimal modifications to the Tri-Bimaximal neutrino mixing*, *JHEP* **11** (2014) 143 [[1405.3022](#)].
- [76] S. Antusch, S.F. King and M. Spinrath, *Spontaneous CP violation in $A_4 \times SU(5)$ with Constrained Sequential Dominance 2*, *Phys. Rev. D* **87** (2013) 096018 [[1301.6764](#)].
- [77] M. Borah, D. Borah and M.K. Das, *Radiative Generation of Non-zero θ_{13} in MSSM with broken A_4 Flavor Symmetry*, *Nucl. Phys. B* **885** (2014) 76 [[1304.0164](#)].
- [78] G.-J. Ding, S.F. King and A.J. Stuart, *Generalised CP and A_4 Family Symmetry*, *JHEP* **12** (2013) 006 [[1307.4212](#)].
- [79] V.V. Vien, *Multiscalar $B - L$ extension with A_4 symmetry for fermion mass and mixing with co-bimaximal scheme*, *Phys. Lett. B* **817** (2021) 136296.
- [80] Y.H. Ahn, S.K. Kang and C.S. Kim, *Spontaneous CP Violation in A_4 Flavor Symmetry and Leptogenesis*, *Phys. Rev. D* **87** (2013) 113012 [[1304.0921](#)].
- [81] D. Aristizabal Sierra and I. de Medeiros Varzielas, *Reactor mixing angle from hybrid neutrino masses*, *JHEP* **07** (2014) 042 [[1404.2529](#)].
- [82] V.V. Vien and H.N. Long, *Neutrino mixing with nonzero θ_{13} and CP violation in the 3-3-1 model based on A_4 flavor symmetry*, *Int. J. Mod. Phys. A* **30** (2015) 1550117 [[1405.4665](#)].
- [83] V.V. Vien, *Cobimaximal neutrino mixing in the $U(1)_{B-L}$ extension with A_4 symmetry*, *Mod. Phys. Lett. A* **35** (2020) 2050311.
- [84] A.E. Cárcamo Hernández and R. Martínez, *A predictive 3-3-1 model with A_4 flavor symmetry*, *Nucl. Phys. B* **905** (2016) 337 [[1501.05937](#)].
- [85] M. Holthausen, M. Lindner and M.A. Schmidt, *Lepton flavor at the electroweak scale: A complete A_4 model*, *Phys. Rev. D* **87** (2013) 033006 [[1211.5143](#)].
- [86] S. Pramanick and A. Raychaudhuri, *A_4 -based seesaw model for realistic neutrino masses and mixing*, *Phys. Rev. D* **93** (2016) 033007 [[1508.02330](#)].
- [87] R. Kalita and D. Borah, *Constraining a type I seesaw model with A_4 flavor symmetry from neutrino data and leptogenesis*, *Phys. Rev. D* **92** (2015) 055012 [[1508.05466](#)].
- [88] S.F. King, S. Morisi, E. Peinado and J.W.F. Valle, *Quark-Lepton Mass Relation in a Realistic A_4 Extension of the Standard Model*, *Phys. Lett. B* **724** (2013) 68 [[1301.7065](#)].
- [89] T. Nomura, Y. Shimizu and T. Yamada, *$A_4 \times U(1)_{PQ}$ model for the lepton flavor structure and the strong CP problem*, *JHEP* **06** (2016) 125 [[1604.07650](#)].
- [90] D. Borah, *Deviations from Tri-Bimaximal Neutrino Mixing Using Type II Seesaw*, *Nucl. Phys. B* **876** (2013) 575 [[1307.2426](#)].
- [91] N. Memenga, W. Rodejohann and H. Zhang, *A_4 flavor symmetry model for Dirac neutrinos and sizable U_{e3}* , *Phys. Rev. D* **87** (2013) 053021 [[1301.2963](#)].

- [92] B. Karmakar and A. Sil, *Nonzero θ_{13} and leptogenesis in a type-I seesaw model with A_4 symmetry*, *Phys. Rev.* **D91** (2015) 013004 [[1407.5826](#)].
- [93] V. Puyam, S.R. Singh and N.N. Singh, *Deviation from Tribimaximal mixing using A_4 flavour model with five extra scalars*, *Nucl. Phys. B* **983** (2022) 115932 [[2204.10122](#)].
- [94] Z.-z. Xing and S. Zhou, *Tri-bimaximal Neutrino Mixing and Flavor-dependent Resonant Leptogenesis*, *Phys. Lett. B* **653** (2007) 278 [[hep-ph/0607302](#)].
- [95] W. Grimus and L. Lavoura, *A Model for trimaximal lepton mixing*, *JHEP* **09** (2008) 106 [[0809.0226](#)].
- [96] E. Ma, *Verifiable radiative seesaw mechanism of neutrino mass and dark matter*, *Phys. Rev. D* **73** (2006) 077301 [[hep-ph/0601225](#)].
- [97] A. Zee, *A Theory of Lepton Number Violation, Neutrino Majorana Mass, and Oscillation*, *Phys. Lett. B* **93** (1980) 389.
- [98] T.P. Cheng and L.-F. Li, *Neutrino Masses, Mixings and Oscillations in $SU(2) \times U(1)$ Models of Electroweak Interactions*, *Phys. Rev. D* **22** (1980) 2860.
- [99] D. Restrepo, O. Zapata and C.E. Yaguna, *Models with radiative neutrino masses and viable dark matter candidates*, *JHEP* **11** (2013) 011 [[1308.3655](#)].
- [100] K.S. Babu, *Model of 'Calculable' Majorana Neutrino Masses*, *Phys. Lett. B* **203** (1988) 132.
- [101] Y. Cai, J. Herrero-García, M.A. Schmidt, A. Vicente and R.R. Volkas, *From the trees to the forest: a review of radiative neutrino mass models*, *Front. in Phys.* **5** (2017) 63 [[1706.08524](#)].
- [102] N. Rojas, R. Srivastava and J.W.F. Valle, *Simplest Scoto-Seesaw Mechanism*, *Phys. Lett. B* **789** (2019) 132 [[1807.11447](#)].
- [103] J. Schechter and J.W.F. Valle, *Neutrinoless Double beta Decay in $SU(2) \times U(1)$ Theories*, *Phys. Rev. D* **25** (1982) 2951.
- [104] S.F. King, *Atmospheric and solar neutrinos with a heavy singlet*, *Phys. Lett. B* **439** (1998) 350 [[hep-ph/9806440](#)].
- [105] S. Antusch, S. Boudjemaa and S.F. King, *Neutrino Mixing Angles in Sequential Dominance to NLO and NNLO*, *JHEP* **09** (2010) 096 [[1003.5498](#)].
- [106] S. Antusch and S.F. King, *Sequential dominance*, *New J. Phys.* **6** (2004) 110 [[hep-ph/0405272](#)].
- [107] S.F. King, *Predicting neutrino parameters from $SO(3)$ family symmetry and quark-lepton unification*, *JHEP* **08** (2005) 105 [[hep-ph/0506297](#)].
- [108] S. Mandal, R. Srivastava and J.W.F. Valle, *The simplest scoto-seesaw model: WIMP dark matter phenomenology and Higgs vacuum stability*, *Phys. Lett. B* **819** (2021) 136458 [[2104.13401](#)].
- [109] D.M. Barreiros, F.R. Joaquim, R. Srivastava and J.W.F. Valle, *Minimal scoto-seesaw mechanism with spontaneous CP violation*, *JHEP* **04** (2021) 249 [[2012.05189](#)].

- [110] Y. Koide, *$S(4)$ flavor symmetry embedded into $SU(3)$ and lepton masses and mixing*, *JHEP* **08** (2007) 086 [0705.2275].
- [111] A. Adulpravitchai, A. Blum and M. Lindner, *Non-Abelian Discrete Groups from the Breaking of Continuous Flavor Symmetries*, *JHEP* **09** (2009) 018 [0907.2332].
- [112] C. Luhn, *Spontaneous breaking of $SU(3)$ to finite family symmetries: a pedestrian's approach*, *JHEP* **03** (2011) 108 [1101.2417].
- [113] A. Merle and R. Zwicky, *Explicit and spontaneous breaking of $SU(3)$ into its finite subgroups*, *JHEP* **02** (2012) 128 [1110.4891].
- [114] B.L. Rachlin and T.W. Kephart, *Spontaneous Breaking of Gauge Groups to Discrete Symmetries*, *JHEP* **08** (2017) 110 [1702.08073].
- [115] S.F. King and Y.-L. Zhou, *Spontaneous breaking of $SO(3)$ to finite family symmetries with supersymmetry - an A_4 model*, *JHEP* **11** (2018) 173 [1809.10292].
- [116] T.J. Burrows and S.F. King, *$A(4)$ Family Symmetry from $SU(5)$ SUSY GUTs in 6d*, *Nucl. Phys. B* **835** (2010) 174 [0909.1433].
- [117] S.F. King, *Unified Models of Neutrinos, Flavour and CP Violation*, *Prog. Part. Nucl. Phys.* **94** (2017) 217 [1701.04413].
- [118] R. de Adelhart Toorop, F. Feruglio and C. Hagedorn, *Finite Modular Groups and Lepton Mixing*, *Nucl. Phys. B* **858** (2012) 437 [1112.1340].
- [119] F. Feruglio, *Are neutrino masses modular forms?*, in *From My Vast Repertoire: Guido Altarelli's Legacy*, A. Levy, S. Forte and G. Ridolfi, eds., pp. 227–266 (2019), DOI [1706.08749].
- [120] F.J. de Anda, S.F. King and E. Perdomo, *$SU(5)$ grand unified theory with A_4 modular symmetry*, *Phys. Rev. D* **101** (2020) 015028 [1812.05620].
- [121] P.P. Novichkov, S.T. Petcov and M. Tanimoto, *Trimaximal Neutrino Mixing from Modular A_4 Invariance with Residual Symmetries*, *Phys. Lett. B* **793** (2019) 247 [1812.11289].
- [122] J.C. Criado and F. Feruglio, *Modular Invariance Faces Precision Neutrino Data*, *SciPost Phys.* **5** (2018) 042 [1807.01125].
- [123] T. Kobayashi, Y. Shimizu, K. Takagi, M. Tanimoto, T.H. Tatsuishi and H. Uchida, *Finite modular subgroups for fermion mass matrices and baryon/lepton number violation*, *Phys. Lett. B* **794** (2019) 114 [1812.11072].
- [124] J.T. Penedo and S.T. Petcov, *Lepton Masses and Mixing from Modular S_4 Symmetry*, *Nucl. Phys. B* **939** (2019) 292 [1806.11040].
- [125] G.-J. Ding, S.F. King and X.-G. Liu, *Neutrino mass and mixing with A_5 modular symmetry*, *Phys. Rev. D* **100** (2019) 115005 [1903.12588].

- [126] D. Borah and B. Karmakar, *A₄ flavour model for Dirac neutrinos: Type I and inverse seesaw*, *Phys. Lett. B* **780** (2018) 461 [[1712.06407](#)].
- [127] D. Borah and B. Karmakar, *Linear seesaw for Dirac neutrinos with A₄ flavour symmetry*, *Phys. Lett. B* **789** (2019) 59 [[1806.10685](#)].
- [128] D. Borah, B. Karmakar and D. Nanda, *Common Origin of Dirac Neutrino Mass and Freeze-in Massive Particle Dark Matter*, *JCAP* **07** (2018) 039 [[1805.11115](#)].
- [129] X.-G. He, Y.-Y. Keum and R.R. Volkas, *A(4) flavor symmetry breaking scheme for understanding quark and neutrino mixing angles*, *JHEP* **04** (2006) 039 [[hep-ph/0601001](#)].
- [130] Y. Lin, *A Predictive A(4) model, Charged Lepton Hierarchy and Tri-bimaximal Sum Rule*, *Nucl. Phys. B* **813** (2009) 91 [[0804.2867](#)].
- [131] M.-C. Chen and S.F. King, *A₄ See-Saw Models and Form Dominance*, *JHEP* **06** (2009) 072 [[0903.0125](#)].
- [132] B. Karmakar and A. Sil, *Spontaneous CP violation in lepton-sector: A common origin for θ_{13} , the Dirac CP phase, and leptogenesis*, *Phys. Rev. D* **93** (2016) 013006 [[1509.07090](#)].
- [133] S. Bhattacharya, B. Karmakar, N. Sahu and A. Sil, *Unifying the flavor origin of dark matter with leptonic nonzero θ_{13}* , *Phys. Rev. D* **93** (2016) 115041 [[1603.04776](#)].
- [134] E. Molinaro and S.T. Petcov, *The Interplay Between the 'Low' and 'High' Energy CP-Violation in Leptogenesis*, *Eur. Phys. J. C* **61** (2009) 93 [[0803.4120](#)].
- [135] G.C. Branco, P.M. Ferreira, L. Lavoura, M.N. Rebelo, M. Sher and J.P. Silva, *Theory and phenomenology of two-Higgs-doublet models*, *Phys. Rept.* **516** (2012) 1 [[1106.0034](#)].
- [136] S.F. King and C. Luhn, *Trimaximal neutrino mixing from vacuum alignment in A₄ and S₄ models*, *JHEP* **09** (2011) 042 [[1107.5332](#)].
- [137] PARTICLE DATA GROUP collaboration, *Review of Particle Physics*, *PTEP* **2020** (2020) 083C01.
- [138] E. Ma, A. Natale and A. Rashed, *Scotogenic A₄ Neutrino Model for Nonzero θ_{13} and Large δ_{CP}* , *Int. J. Mod. Phys. A* **27** (2012) 1250134 [[1206.1570](#)].
- [139] D. Hernandez and A.Y. Smirnov, *Lepton mixing and discrete symmetries*, *Phys. Rev. D* **86** (2012) 053014 [[1204.0445](#)].
- [140] M. Tanimoto, *Neutrinos and flavor symmetries*, *AIP Conf. Proc.* **1666** (2015) 120002.
- [141] Y. Shimizu, M. Tanimoto and K. Yamamoto, *Predicting CP violation in Deviation from Tri-bimaximal mixing of Neutrinos*, *Mod. Phys. Lett. A* **30** (2015) 1550002 [[1405.1521](#)].
- [142] I. Esteban, M. Gonzalez-Garcia, M. Maltoni, T. Schwetz and A. Zhou, *The fate of hints: updated global analysis of three-flavor neutrino oscillations*, *JHEP* **09** (2020) 178 [[2007.14792](#)].
- [143] F. Capozzi, E. Di Valentino, E. Lisi, A. Marrone, A. Melchiorri and A. Palazzo, *Unfinished fabric of the three neutrino paradigm*, *Phys. Rev. D* **104** (2021) 083031 [[2107.00532](#)].

- [144] W. Rodejohann and J.W.F. Valle, *Symmetrical Parametrizations of the Lepton Mixing Matrix*, *Phys. Rev. D* **84** (2011) 073011 [[1108.3484](#)].
- [145] PARTICLE DATA GROUP collaboration, *Review of Particle Physics*, *PTEP* **2020** (2020) 083C01.
- [146] KAMLAND-ZEN collaboration, *Search for Majorana Neutrinos near the Inverted Mass Hierarchy Region with KamLAND-Zen*, *Phys. Rev. Lett.* **117** (2016) 082503 [[1605.02889](#)].
- [147] GERDA collaboration, *Improved Limit on Neutrinoless Double- β Decay of ^{76}Ge from GERDA Phase II*, *Phys. Rev. Lett.* **120** (2018) 132503 [[1803.11100](#)].
- [148] LEGEND collaboration, *The Large Enriched Germanium Experiment for Neutrinoless $\beta\beta$ Decay: LEGEND-1000 Preconceptual Design Report*, [2107.11462](#).
- [149] NEXO collaboration, *nEXO: neutrinoless double beta decay search beyond 10^{28} year half-life sensitivity*, *J. Phys. G* **49** (2022) 015104 [[2106.16243](#)].
- [150] T. Toma and A. Vicente, *Lepton Flavor Violation in the Scotogenic Model*, *JHEP* **01** (2014) 160 [[1312.2840](#)].
- [151] A. Vicente and C.E. Yaguna, *Probing the scotogenic model with lepton flavor violating processes*, *JHEP* **02** (2015) 144 [[1412.2545](#)].
- [152] C. Hagedorn, J. Herrero-García, E. Molinaro and M.A. Schmidt, *Phenomenology of the Generalised Scotogenic Model with Fermionic Dark Matter*, *JHEP* **11** (2018) 103 [[1804.04117](#)].
- [153] T. Aushev et al., *Physics at Super B Factory*, [1002.5012](#).
- [154] A. Ilakovac and A. Pilaftsis, *Flavor violating charged lepton decays in seesaw-type models*, *Nucl. Phys. B* **437** (1995) 491 [[hep-ph/9403398](#)].
- [155] D. Tommasini, G. Barenboim, J. Bernabeu and C. Jarlskog, *Nondecoupling of heavy neutrinos and lepton flavor violation*, *Nucl. Phys. B* **444** (1995) 451 [[hep-ph/9503228](#)].
- [156] D.N. Dinh, A. Ibarra, E. Molinaro and S.T. Petcov, *The $\mu - e$ Conversion in Nuclei, $\mu \rightarrow e\gamma, \mu \rightarrow 3e$ Decays and TeV Scale See-Saw Scenarios of Neutrino Mass Generation*, *JHEP* **08** (2012) 125 [[1205.4671](#)].
- [157] G. Bambhaniya, P.S. Bhupal Dev, S. Goswami, S. Khan and W. Rodejohann, *Naturalness, Vacuum Stability and Leptogenesis in the Minimal Seesaw Model*, *Phys. Rev. D* **95** (2017) 095016 [[1611.03827](#)].
- [158] P. Ghosh, A.K. Saha and A. Sil, *Study of Electroweak Vacuum Stability from Extended Higgs Portal of Dark Matter and Neutrinos*, *Phys. Rev. D* **97** (2018) 075034 [[1706.04931](#)].
- [159] MEG collaboration, *Search for the lepton flavour violating decay $\mu^+ \rightarrow e^+\gamma$ with the full dataset of the MEG experiment*, *Eur. Phys. J. C* **76** (2016) 434 [[1605.05081](#)].
- [160] MEG II collaboration, *The design of the MEG II experiment*, *Eur. Phys. J. C* **78** (2018) 380 [[1801.04688](#)].

- [161] E.M. Dolle and S. Su, *The Inert Dark Matter*, *Phys. Rev. D* **80** (2009) 055012 [[0906.1609](#)].
- [162] PLANCK collaboration, *Planck 2018 results. VI. Cosmological parameters*, *Astron. Astrophys.* **641** (2020) A6 [[1807.06209](#)].
- [163] CMS collaboration, *Search for invisible decays of the Higgs boson produced via vector boson fusion in proton-proton collisions at $\sqrt{s} = 13$ TeV*, *Phys. Rev. D* **105** (2022) 092007 [[2201.11585](#)].